Downsystem Grain-Size Trends and Mass Balance of an Ancient Wave-Influenced Sediment Routing System: Middle Jurassic Brent Delta, Northern North Sea, Offshore UK and Norway

Ikenna C. Okwara[1,2], Gary J. Hampson*[1], Alexander C. Whittaker[1] and Gareth G. Roberts[1]

[1]Department of Earth Science and Engineering, Imperial College London, London SW7 2AZ, U.K.

[2] Department of Geology, University of Nigeria, Nsukka, Nigeria

Author note

Ikenna C. Okwara

Gary J. Hampson https://orcid.org/0000-0003-2047-8469

Alexander C. Whittaker

Gareth G. Roberts

This manuscript is a non-peer reviewed preprint submitted to EarthArXiv. The manuscript has also been submitted for peer review to the journal *Sedimentologika*.

Correspondence concerning this article should be addressed to Gary Hampson, Imperial College London, London SW7 2AZ, U.K. Email: g.j.hampson@imperial.ac.uk

ABSTRACT

We reconstruct upsystem-to-downsystem grain-size variations in the sediment routing systems of the data-rich Middle Jurassic Brent Group of the northern North Sea, using published stratigraphic, thickness, palaeogeographic, provenance and age constraints combined with representative core and wireline-log data. Facies associations provide a textural proxy for gravel, sand and mud grain-size fractions, and their distributions define spatio-temporal variations in grain size within four previously documented genetic sequences (J22, J24, J26, J32). Sediment was sourced from the west (Shetland Platform), east (Norwegian Landmass) and south (Mid-North Sea High). The corresponding sediment routing systems were geographically distinct in the oldest (J22) and youngest (J32) genetic sequences, but combined to feed a large wave-dominated delta ('Brent Delta') in genetic sequences J24 and J26.

Few of the Brent Group sediment routing systems exhibit the downsystem-fining grain-size trend predicted by sediment mass balance theory. Deviations from this reference trend reflect: (1) sparse sampling of channelised fluvial and fluvio-tidal sandbodies in upsystem locations; (2) preferential trapping of sand in underfilled antecedent and syn-depositional, half-graben depocentres in genetic sequences J22 and J32; and (3) nearshore retention of sand by shoaling waves in wave-dominated shoreface and barrier-strandplain systems. This third type of deviation reveals that spatial facies partitioning due to shallow-marine process regime distorts the simple downsystem-fining reference trend, and supports the interpretation that large volumes of predominantly muddy sediment were bypassed beyond the 'Brent Delta'

into neighbouring basins. In summary, our analysis demonstrates a practical tool to interpret sediment supply and sediment dispersal in the stratigraphic record.

[end of abstract]

Keywords: sediment grain size, sediment mass-balance; sediment routing system; source-to-sink; Brent Group

1. Introduction

Sediment supply and accommodation space are widely considered to be the two principal controls on stratigraphic architecture (e.g. Posamentier and Vail, 1988; Catuneanu et al., 2009; Allen et al., 2013; Romans et al., 2016). For instance, coupled landscape-basin models (e.g. Armitage et al., 2011) clearly show how changing sediment supply as opposed to changing accommodation-space generation should give rise to distinct stratigraphic signatures. The role of sediment supply is often more difficult to constrain than that of accommodation space, with the result that sediment supply is rarely explicitly interpreted in studies of stratigraphic architecture (e.g. Heller et al., 1993; Galloway, 2001; Brommer et al., 2009; Hampson, 2016; Burgess and Steel, 2017; Zhang et al., 2019). In contrast, source-to-sink studies have developed several approaches to interpreting sediment flux from geologic or geomorphic data sets over the last two decades, and these have been applied to constraining sediment supply in the stratigraphic record. Such source-to-sink approaches include the empirical BQART model of sediment load applied to modern or palaeo-catchments (Syvitski and Milliman, 2007; Zhang et al., 2018; Watkins et al., 2019; Lyster et al., 2020), empirical geomorphological scaling relationships (Sømme et al., 2009; Nyberg et al., 2018; Snedden et al., 2018), and

the “fulcrum” palaeohydrological scaling model applied to stratigraphic observations (Holbrook and Wanas, 2014; Bhattacharya et al., 2016). These approaches to estimating sediment flux have been argued to show broad consistency with each other, and with mapped sediment volumes and ages in rich datasets from the stratigraphic record (Brewer at al., 2020; Lyster et al., 2020; Heins, 2023). However many of these studies to date have not incorporated the insights that can be gleaned from facies-based grain-size data (e.g. Reynolds, 2019). Preferential deposition of coarser grains during sediment transport gives rise to downsystem-fining trends in stratigraphic grain size that can provide a reference for comparison between sediment routing systems when normalised with respect to accommodation space (i.e. ‘sediment mass balance ‘; Fig. 1; Strong et al., 2005; Whittaker et al., 2011; Paola and Martin, 2012; Michael et al., 2013, 2014; Hampson et al., 2014). Thus, downsystem-fining trends in grain size can in principle be used in combination with sediment flux estimates and, potentially, provenance constraints on the grain-size mix of supplied sediment to infer spatio-temporal variations in sediment supply. The extent to which facies partitioning may complicate spatial interpretations of grain size trends remains contentious (c.f. Michael et al., 2013, 2014), but its use offers the means to apply facies-based sequence stratigraphic analysis to constrain the role of sediment supply on stratigraphic architecture and sediment routing and dispersal (Fig. 1).

In this paper, we reconstruct downsystem variations in grain size within a sediment mass balance context for the well-documented, data-rich sediment routing systems of the Middle Jurassic Brent Group, in order to constrain sediment supply to these systems and to assess potential sediment bypass basinward of the wave-dominated

‘Brent Delta’. This work extends the sediment mass balance analysis of the ‘Brent Delta’ sediment routing system(s) presented in Okwara et al. (2023), which is based on the same dataset. The specific aims of the paper are threefold: (1) to document downsystem variations in grain size in sediment routing systems of the Middle Jurassic Brent Group, normalised with respect to accommodation space due to tectonic subsidence; (2) to reconstruct the flux and grain-size composition of sediment supplied to these sediment routing systems; and (3) to compare these results to estimates of sediment supply derived from the BQART sediment-load model (Okwara et al., 2023) and to qualitative constraints from facies models and sequence stratigraphic interpretations of the ‘Brent Delta’ (e.g. Budding and Inglin, 1981; Scott, 1992; Johannessen et al., 1995; Olsen and Steel, 1995; Løseth and Ryseth, 2003; Went et al., 2013). Our analysis serves to illustrate the pragmatic application of downsystem-fining and sediment mass balance concepts to the stratigraphic record, including interpretive insights and limitations.

2. Geological Setting

2.1. Tectono-stratigraphic and Climatic Context

The Middle Jurassic Brent Group and associated strata were deposited in the northern part of the North Sea, within a north-south-trending depocentre that subsequently developed into the Viking Graben and Horda Platform (Fig. 2A, B; e.g. Husmo et al., 2003). The proto-Viking Graben depocentre is bounded by the Shetland Platform to the west, Norwegian Landmass to the east, and Mid-North Sea High to the south (Fig. 2B).

The proto-Viking Graben was initiated during Late Permian to Early Triassic rifting (Barton and Wood, 1984; Steel and Ryseth, 1990; Færseth, 1996; Zanella and Coward, 2003; Duffy et al., 2015), and underwent post-rift thermal subsidence during Late Triassic to Middle Jurassic times (Partington et al., 1993; Rattey and Hayward, 1993; Steel, 1993) (Fig. 2C). Middle Jurassic thermal doming and uplift of the Mid-North Sea, south of the proto-Viking Graben, resulted in erosion of Triassic to Lower Jurassic strata here, and the development of an intra-Aalenian unconformity, widely referred to as the 'mid-Cimmerian Unconformity' (Fig. 2B, C; Ziegler, 1990; Underhill and Partington, 1993, 1994). Middle to Late Jurassic strata onlap this unconformity, recording later collapse of the dome (Underhill and Partington, 1993, 1994; Husmo et al., 2003). Subsequent Late Jurassic to Early Cretaceous rifting resulted in development of the trilete North Sea rift, and established the present-day configuration of structural elements, including the Viking Graben and Horda Platform (e.g. Underhill and Partington, 1993; Zanella and Coward, 2003). In the developing Viking Graben, Late Jurassic to Early Cretaceous rifting reactivated some north-south-trending, Permo-Triassic rift faults and generated additional northeast-southwest-trending faults (Færseth, 1996; Zanella and Coward, 2003; Duffy et al., 2015; Phillips et al., 2019).

The proto-Viking Graben depocentre occupied a palaeo-latitude of c. 44-48°N during the Middle Jurassic (Fig. 2A; Ziegler, 1990; Torsvik et al., 2002). Coal petrology, palynological data, palaeo-latitude reconstructions, strontium isotope data, oxygen isotope data, and ocean-atmosphere numerical models indicate that the depocentre was subject to a sub-tropical and humid climate throughout the Middle Jurassic, with

mean annual temperature estimated to have been ca. 20°C (Abbink et al., 2001; Sellwood and Valdes, 2006, 2008; Prokoph et al., 2008).

2.2. Stratigraphic and Palaeogeographic Framework of 'Brent Delta' Sediment Routing System(s)

The stratigraphic and palaeogeographic framework of the Brent Group and related strata have been documented in many regional, basin-scale studies (e.g. Graue et al., 1987; Helland-Hansen et al., 1992; Mitchener et al., 1992; Johannessen et al., 1995; Sneider et al., 1995; Fjellanger et al., 1996; Hampson et al., 2004). These studies extended previous sedimentological facies analysis and models (e.g. Budding and Inglin, 1981; Richards and Brown, 1986; Livera, 1989; Livera and Caline, 1990; Scott, 1992; Muto and Steel, 1997) to develop sequence stratigraphic interpretations calibrated to biostratigraphic data (e.g. Whitaker et al., 1992; Partington et al., 1993). Palaeogeographies were reconstructed for specific sequence stratigraphic intervals. The resulting sedimentological, stratigraphic and palaeogeographic frameworks are broadly consistent with each other, such that they can be readily synthesised (e.g. Okwara et al., 2023); components of these frameworks are described in more detail below, in Steps 1-5 of the Method section.

Petrographic data (e.g. Morton, 1985, 1992; Hamilton et al., 1987; Hurst and Morton, 1988; Mearns, 1992) and palaeogeographic reconstructions (e.g. Mitchener et al., 1992; Fjellanger et al., 1996; Husmo et al., 2003) indicate that sediment was routed into the deposits of the Brent Group from three main source areas at the margins of the proto-Viking Graben: the Shetland Platform, Norwegian Landmass, and Mid-North Sea High (Fig. 2B; e.g. Okwara et al., 2023). The Shetland Platform lay to the

west (Fig. 2B), was composed mainly of Devonian, Carboniferous and Permo-Triassic sedimentary rocks reworked from Caledonian metamorphic basement (Zanella and Coward, 2003; Morton et al., 2004), and is tentatively estimated to have had a Middle Jurassic palaeorelief of 1 km (Okwara et al., 2023). The Norwegian Landmass lay to the east (Fig. 2B), was composed of Precambrian and Caledonian metamorphic basement (Husmo et al., 2003; Morton et al., 2004), and had palaeorelief of 1-1.2 km during the Middle Jurassic (Gabrielsen et al., 2010; Medvedev and Hartz, 2015). The Mid-North Sea High lay to the south (Fig. 2B), was composed of sandstone-dominated Triassic and mudstone-dominated Lower Jurassic sedimentary rocks eroded at the 'mid-Cimmerian Unconformity' (Fig. 2B, C; Ziegler, 1990; Underhill and Partington, 1993, 1994), and had a Middle Jurassic palaeorelief of 0.3-0.5 km (Underhill and Partington, 1993; Okwara et al., 2023).

In the lowermost (cf. Broom and Oseberg formations; genetic sequence J22 in Fig. 3) and uppermost Brent Group (cf. Tarbert Formation; genetic sequence J32 in Fig. 3), deposition was confined to the margins of the proto-Viking Graben and three distinct groups of sediment routing systems are evident in palaeogeographic reconstructions. These sediment routing systems fed fan-delta shorelines in the lowermost Brent Group (e.g. Muto and Steel, 1997), and a wide range of shoreline types, including wave-dominated barrier islands and strandplains, in the uppermost Brent Group (e.g. Hampson et al., 2004). In the middle Brent Group (cf. Rannoch, Etive and Ness formations; genetic sequences J24 and J26 in Fig. 3), these sediment routing systems combined in the central axis of the proto-Viking Graben to feed wave-dominated barrier island and strandplain shorelines of the 'Brent Delta' (e.g. Budding and Inglin, 1981).

3. Dataset and Method

3.1. Dataset

We use data from 84 representative exploration wells (Fig. 4, Table 1), each of which has previously been interpreted within one of four regional genetic stratigraphic and sequence stratigraphic frameworks (Mitchener et al., 1992; Sneider et al., 1995; Fjellanger et al., 1996; Hampson et al., 2004; Fig. 3). These four frameworks are compatible with each other, and use many of the same regional and sub-regional stratigraphic surfaces to define genetic stratigraphic and sequence stratigraphic units. In this context, we use four of the “J sequences” proposed by Mitchener et al. (1992) as the stratigraphic intervals in our analysis (J22, J24, J26 and J32 in Fig. 3; see also Okwara et al., 2023). Each “J sequence” is a genetic sequence (*sensu* Galloway, 1989) bounded by biostratigraphically calibrated maximum flooding surfaces of basinwide extent (Partington et al., 1993).

Wells were selected based on their geographical distribution (Fig. 4B), their use in existing regional genetic stratigraphic and sequence stratigraphic frameworks (Mitchener et al., 1992; Sneider et al., 1995; Fjellanger et al., 1996; Hampson et al., 2004; Fig. 3, Table 1), and their previously interpreted sedimentological character (Mitchener et al., 1992; Sneider et al., 1995; Fjellanger et al., 1996; Hampson et al., 2004), such that they capture the full range of facies associations in the ‘Brent Delta’ sediment routing system(s). In parts of the study area that contain many closely spaced fields with Brent Group reservoirs (e.g. the southern part of UK quadrant 211 and northern part of UK quadrant 3; Fig. 4B), we were able to select wells from a

large number of candidates. Other parts of the study area contain only few wells that penetrate Middle Jurassic strata (e.g. UK quadrant 9 and Norwegian quadrants 24 and 25; Fig. 4B). Approximately 1360 m of core from eight of the 84 studied wells (Table 2) was described using sedimentological facies analysis, in order to define the overall lithological and grain-size characteristics of facies associations (see also Okwara et al., 2023). Core descriptions were also used to interpret facies associations in, and thereby calibrate the lithological composition of, uncored intervals and wells (see also Okwara et al., 2023).

The thicknesses of the J22, J24, J26 and J32 genetic sequences (Fig. 3) between the studied wells were generated by interpreting contours between studied well data points, with additional constraints provided by published isopach maps of the J24, J26 and J32 genetic sequences (Mitchener et al., 1992) and Lower-to-Middle Jurassic strata (Husmo et al., 2003), both of which are derived from well and seismic data. We include only detrital siliciclastic sediment in our thickness estimates, and exclude coals, which are produced *in situ* biogenically. Gross facies-association distributions in the J22, J24, J26 and J32 genetic sequences (Fig. 3) in between the studied wells were taken from published palaeogeographic maps (Mitchener et al., 1992; Fjellanger et al., 1996; Husmo et al., 2003), and are used to define the routing of sediment derived from the Shetland Platform, Norwegian Landmass and Mid-North Sea High source areas (Ziegler 1990; Underhill and Partington, 1993).

3.2. Method

We used the method of Hampson et al. (2014) to characterise downsystem trends in grain size; this method was adapted from those of Barnes and Heins (2009),

Brommer et al. (2009), Carvajal and Steel (2012), and Michael at el. (2013, 2014a). The method has eight steps, each of which are described below together with the data that underlie their implementation. The method and its results are complementary to the sediment mass balance analysis of the 'Brent Delta' sediment routing system(s) presented in Okwara et al. (2023) and based on the same dataset. Okwara et al. (2023) characterised the net-depositional sediment mass and age model (i.e. depositional-sink sediment budget) of the J22, J24, J26 and J32 genetic sequences (Fig. 3) and the sediment mass supplied to the combined J22-J32 interval by sediment source areas (i.e. source-area sediment budget), using the BQART sediment load model and independent geometrical reconstruction of eroded volumes. Their key result was that the depositional-sink sediment budget was an order-of-magnitude smaller than the source-area sediment budget, implying that there was significant sediment dispersal from the 'Brent Delta' sediment routing system(s) by alongshore transport and/or down-dip bypass into coeval depocentres (cf. Fig. 1). Here we extend the analysis of Okwara et al. (2023) by characterising downsystem trends in grain size within the net-depositional sediment mass of the J22, J24, J26 and J32 genetic sequences. We do not repeat their uncertainty analysis of net-depositional sediment mass, but instead address uncertainty in the upsystem-to-downsystem partitioning of grain-size fractions in the net-depositional sediment mass of the J22, J24, J26 and J32 genetic sequences.

3.2.1 Step 1: Definition of Stratigraphic Intervals

The stratigraphic framework used in this study is summarised in Figure 3. Our analysis is formulated for four stratigraphic intervals, which correspond to the J22, J24, J26 and J32 genetic sequences of Mitchener et al. (1992). Each sequence is

outlined below, and illustrated via isopach and palaeogeographic maps (Figs. 5-8), core and wireline logs from representative wells (Fig. 9), and well correlation panels (Fig. 10).

The base of the J22 genetic sequence is defined regionally by a maximum flooding surface that is calibrated using palynological data to the Levesquei ammonite zone (Fig. 3; Partington et al., 1993). However, an unconformity (sequence boundary) marked by an abrupt basinward shift of facies-association belts at the base of the Broom and Oseberg formations indicates that this maximum flooding surface has been removed over much of the northern North Sea (Mitchener et al., 1992; SB177 of Fjellanger et al., 1996; SB100 of Hampson et al., 2004). The J22 genetic sequence is characterised by: (1) regression and subsequent transgression of fluvio-estuarine channels and weakly wave-influenced (bioturbated) shorefaces, comprising the Broom Formation, from the western basin margin (Figs. 5B, 9A, C, 10A; e.g. Mitchener et al., 1992; Hampson et al., 2004); (2) regression and subsequent transgression of fluvio-estuarine channels and fan deltas, comprising the Oseberg Formation, from the eastern basin margin (Figs. 5B, 9B, 10B; e.g. Mitchener et al., 1992; Sneider et al., 1995; Fjellanger et al., 1996); and (3) accumulation of coastal plain strata, including the Bruce ‘C’ Sands, and minor northward shoreline regression and subsequent transgression in the southernmost basin axis (Figs. 5B, 10C; e.g. Mitchener et al., 1992). The top of the J22 genetic sequence is defined regionally by the J24 maximum flooding surface, which was developed in the Levesquei ammonite zone (Fig. 3; Partington et al., 1993; MFS170 of Fjellanger et al., 1996; FS200 of Hampson et al., 2004). This maximum flooding

surface corresponds to a thick (5-10 m), laterally extensive coal seam (Bruce B-C Coal; e.g. Mitchener et al., 1992).

The J24 genetic sequence is defined at its base by the J24 maximum flooding surface (Fig. 3; Partington et al., 1993; MFS170 of Fjellanger et al., 1996; FS200 of Hampson et al., 2004), and is characterised by northward regression along the basin axis of a wave-dominated shoreface and barrier bar (Rannoch and Etive formations) and associated coastal plain, lagoon and fluvio-estuarine channels (lower Ness Formation) (Figs. 6B, 9, 10; e.g. Mitchener et al., 1992; Sneider et al., 1995; Fjellanger et al., 1996; Husmo et al., 2003; Hampson et al., 2004). The top of the J24 genetic sequence is defined regionally by the J26 maximum flooding surface, occurring in the Garantiana ammonite zone and marked by the base of the laterally extensive, marginal-marine 'Mid Ness Shale' (Fig. 3; Partington et al., 1993; MFS167 of Fjellanger et al., 1996; FS400 of Hampson et al., 2004).

The base of the J26 genetic sequence is defined by the J26 maximum flooding surface (Fig. 3; Partington et al., 1993; MFS167 of Fjellanger et al., 1996; FS400 of Hampson et al., 2004). The J26 genetic sequence is characterised by continued, minor northward regression followed by aggradation and subsequent transgression of wave-dominated shorefaces and barrier bars (Etive and, locally, Tarbert formations), coastal plains, lagoons and fluvio-estuarine channels (upper Ness Formation, Bruce 'B' Sands) (Figs. 7B, 9, 10; e.g. Mitchener et al., 1992; Sneider et al., 1995; Fjellanger et al., 1996; Husmo et al., 2003; Hampson et al., 2004). The top of the J26 genetic sequence is defined regionally by the J32 maximum flooding surface, developed in the Parkinsoni ammonite zone (Fig. 3; Partington et al., 1993;

MFS165 of Fjellanger et al., 1996). A sub-regional unconformity (sequence boundary; SB1000 of Hampson et al., 2004) indicates that this maximum flooding surface has been removed near the western basin margin.

The base of the J32 genetic sequence is defined by the J32 maximum flooding surface (Fig. 3; Partington et al., 1993; MFS165 of Fjellanger et al., 1996) and a sub-regional unconformity (SB1000 of Hampson et al., 2004). The J32 genetic sequence is characterised by net-transgressive stacking of a range of shallow- and marginal-marine deposits, including fluvio-estuarine channels and fan deltas, weakly wave-influenced (bioturbated) shorefaces, wave-dominated shorefaces (Tarbert Formation, Bruce 'A' Sands and Hugin Formation) and offshore mudstones (Heather Formation), which overlie aggradational coastal-plain and lagoonal deposits (upper Ness Formation and Sleipner Formation) (Figs. 8B, 9, 10; e.g. Mitchener et al., 1992; Sneider et al., 1995; Fjellanger et al., 1996; Husmo et al., 2003; Hampson et al., 2004). Palaeoshorelines near the base of the J32 genetic sequence were oriented west-east (cf. Fig. 7B), but evolved to a north-south orientation, parallel to major fault trends in the basin, as they retreated towards the basin margins (Fig. 8B). The top of the J32 genetic sequence is defined regionally by the J34 maximum flooding surface of Mitchener et al. (1992), which is calibrated using palynological data to the Discus ammonite zone (Fig. 3; J36 maximum flooding surface of Partington et al., 1993; MFS157 of Fjellanger et al., 1996). Published local revisions to biostratigraphic picks and the interpreted J34 maximum flooding surface of Mitchener et al. (1992) are incorporated into our stratigraphic correlations (Fig. 10); notably, the J32 genetic sequence is interpreted to occur at greater depths, predominantly within the coastal-plain and lagoonal deposits of the Sleipner Formation, in Norwegian quadrant 15

(after the revised biostratigraphic framework used in Kieft et al., 2011; e.g. well 15/3-3 in Fig. 10C).

3.2.2 Step 2: Thicknesses and areal extents of Stratigraphic Intervals

The thicknesses and areal extents of the J22, J24, J26 and J32 genetic sequences (Fig. 3) away from the studied wells were generated by interpreting thickness contours between studied well data points using published regional isopach maps of the J24, J26 and J32 genetic sequences (Mitchener et al., 1992) and Lower-to-Middle Jurassic strata (Husmo et al., 2003), both of which are derived from well and seismic data without accounting for compaction. Thickness changes in the J22 genetic sequence (Fig. 5A) are relatively small. They are either confined to the hangingwalls of a few extensional faults or occur above deeply buried, fault-bounded depocentres developed during Lower Triassic rifting (Fig. 2C). The former are aligned sub-parallel to palaeoshoreline trends (Fig. 5B), suggesting that the hangingwall depocentres of these extensional faults were underfilled prior to, and thus influenced deposition of, the J22 genetic sequence (e.g. Mitchener et al., 1992; Hampson et al., 2004). In the J24 and J26 genetic sequences (Figs. 6A, 7A), thickness changes are similarly confined to the hangingwalls of a few extensional faults and to locations above deeply buried Lower Triassic depocentres (e.g. Folkestad et al., 2014). Palaeoshorelines were oriented approximately west-east (Figs. 6B, 7B). Their orientation is nearly perpendicular to, and continues across, syn-depositional extensional faults (Figs. 6B, 7B), suggesting that the associated depocentres were filled and/or overfilled. The J24 and J26 genetic sequences both thin northward of the maxiumum-regressive palaeoshoreline position (Figs. 6, 7), reflecting underfilling of relatively deep bathymetry offshore of these

palaeoshorelines. The J32 genetic sequence records the initiation of Upper Jurassic rifting (Figs. 2C, 3), which is expressed as pronounced thickening into the hangingwalls of extensional faults as they propagated and linked (Fig. 8A; e.g. Davies et al., 2000; McLeod et al., 2000), significant time gaps across unconformities confined to footwall crests and rift shoulders, onlap on to rift-generated topography, and the extrusion of volcanic rocks on the Mid-North Sea High (e.g. Mitchener et al., 1992; Quirie et al., 2019). Deflection of palaeoshorelines to a north-south orientation, parallel to major extensional fault trends in the basin (Fig. 8B), is consistent with the development of underfilled hangingwall depocentres during the upper part of the J22 genetic sequence, as Upper Jurasic rifting continued (Fig. 3). Revised correlation of the J32 genetic sequence in Norwegian quadrant 15 (after the biostratigraphic framework used in Kieft et al., 2011; e.g. well 15/3-3 in Fig. 10C) greatly reduces (by over 100 m locally) the thickness of this genetic sequence in the southernmost part of the study area (Fig. 8B) compared to the thickness interpreted by Mitchener et al. (1992; their figure 10).

3.2.3 Step 3: Formulation of an Age Model

The boundaries of the J22, J24, J26 and J32 genetic sequences have been assigned absolute ages and durations based on calibrating ammonite zones to radiometric age data in the geological time scale of Gradstein et al. (2012) and Ogg et al. (2016) (Fig. 3; see also Okwara et al., 2023). This age model reduces the total duration represented by Aalenian-to-Bathonian strata from 22 Myr (Mitchener et al., 1992) to 8 Myr (Ogg et al., 2016), with an uncertainty of ±0.5-0.7 Myr in the duration of individual genetic sequences (Okwara et al., 2023).

3.2.4 Step 4: Delineation of Sediment Routing System(s) in each Stratigraphic Interval

Palaeogeographic reconstructions (Figs. 5B, 6B, 7B, 8B; e.g. Mitchener et al., 1992; Fjellanger et al., 1996; Husmo et al., 2003), detrital heavy mineral (e.g. garnet) geochemistry and isotope (e.g. strontium-neodymium) data (e.g. Morton, 1985, 1992; Hamilton et al., 1987; Hurst and Morton, 1988; Mearns, 1992) indicate that sediment was supplied from three main source areas: the Shetland Platform to the west, Norwegian Landmass to the east, and Mid-North Sea High to the south (e.g. Okwara et al., 2023). In the J22 and J32 genetic sequences, palaeoshorelines adjacent to the western, eastern and southern basin margins are palaeogeographically distinct (Figs. 5B, 8B), such that we interpret a sediment routing system (or a combined group of closely spaced sediment routing systems) lying directly downsystem of, and fed by, each source area. For these genetic sequences, we account for the sediment mass and downsystem grain-size trends in each of the three sediment routing systems (indicated by the red boxes labelled “Fig. 12A, B, C” in Fig. 5B, and “Fig. 12F, G, H” in Fig. 8B). In the J24 and J26 genetic sequences, the three sediment routing systems are interpreted to combine, such that they fed a single west-east-trending palaeoshoreline (Figs. 6B, 7B). For these genetic sequences, we can only analyse the combined sediment routing system (indicated by the red boxes labelled “Fig. 12D” in Fig. 6B, and “Fig. 12E” in Fig. 7B).

We do not subdivide the sediment routing systems into component segments (cf. “sediment storage compartments” of Carvajal and Steel, 2012) defined by major facies-association belts (e.g. Hampson et al., 2014) and/or geomorphological breaks in slope (e.g. Sømme et al., 2009) in our analysis, because facies-association

boundaries extend over large upsystem-to-downsystem distances due to regression and transgression of the sediment routing system(s) in each genetic sequence (Fig. 10) and geomorphological breaks in slope are not resolved by the thickness variations of genetic sequences in our well-based dataset.

3.2.5 Step 5: Construction of a Facies-Association Scheme as a Proxy for Grain-Size Distributions

We use a facies-association classification scheme compiled from previous sedimentological studies of the Brent Group (Budding and Inglin, 1981; Richards and Brown, 1986; Graue et al., 1987; Livera, 1989; Ryseth, 1989; Livera and Caline, 1990; Mitchener et al., 1992; Scott, 1992; Johannessen et al., 1995; Fjellanger et al., 1996; Muto and Steel, 1997; Løseth and Ryseth, 2003; Morris et al., 2003; Hampson et al., 2004) to characterise lithology and grain-size distributions in deposits of the sediment routing system(s) in each genetic sequence. This facies-association scheme is summarised in Table 3, illustrated in representative cored wells (Fig. 9) and correlation panels (Fig. 10), and explained in more detail in the Supplementary Material of Okwara et al., 2023). The scheme comprises three coastal-plain facies associations, three marginal-marine facies associations, and four shallow-marine facies associations. Our work, and that of previous authors, which is compiled in the facies-association scheme, is based on facies analysis of core incorporatingqualitative descriptions of the grain size and sorting characteristics of each facies association. These grain-size characteristics are not documented to vary systematically with downsystem distance in any of the facies associations, such that each facies association provides a measure of lithology and grain size that is independent of upsystem-to-downsystem position (cf. Hampson et al., 2014). We

therefore assume that variations in the proportion of facies associations from upsystem to downsystem are a sufficient first-order descriptor of trends in grain size at the scale of the sediment routing system (i.e. “architectural fining” of Hampson et al., 2014). The proportion of gravel, sand and mud grain-size classes that is defined by qualitative descriptions of each facies association is summarised in Table 3.

Facies associations in uncored wells and intervals are interpreted using wireline-log characteristics, particularly gamma ray, neutron, density and sonic logs (Table 3). Our wireline-log interpretations of facies associations are consistent with previous Brent Group studies using similar wireline-log data (Budding and Inglin, 1981; Richards and Brown, 1986; Graue et al., 1987; Livera, 1989; Ryseth, 1989; Livera and Caline, 1990; Mitchener et al., 1992; Scott, 1992; Johannessen et al., 1995; Fjellanger et al., 1996; Muto and Steel, 1997; Løseth and Ryseth, 2003; Morris et al., 2003; Hampson et al., 2004).

3.2.6 Step 6: Calculation of Facies-Association and Grain-Size Volumes in Sediment Routing System(s)

The present-day, compacted volume of preserved deposits for each sediment routing system in each stratigraphic interval, as identified in step 4 above, was calculated from the appropriate area of the isopach map for that stratigraphic interval (i.e. indicated by the red boxes labelled “Fig. 12A, B, C” in Fig. 5A, “Fig. 12D” in Fig. 6A, “Fig. 12E” in Fig. 7A, and “Fig. 12F, G, H” in Fig. 8A). The fractions of these sediment volumes that are composed of different facies associations (Table 3) and of gravel, sand and mud grain size classes were estimated from the studied well data (Fig. 4), as outlined below.

For each sediment routing system in each stratigraphic interval the following proximal-to-distal transects were constructed: (1) west to east transect for systems fed from the Shetland Platform (in red boxes labelled “Fig. 12A” in Fig. 5 and “Fig. 12F,” in Fig. 8); (2) east to west transect for systems fed from the Norwegian Landmass (in red boxes labelled “Fig. 12B” in Fig. 5 and “Fig. 12G” in Fig. 8); and (3) south to north transect for systems fed from the Mid-North Sea High (in red boxes labelled “Fig. 12C” in Fig. 5 and “Fig. 12H” in Fig. 8) or the combination of all three sediment source areas (in red boxes labelled “Fig. 12D” in Fig. 6 and “Fig. 12E” in Fig. 7). Wells and groups of wells that are closely spaced along depositional strike (i.e. perpendicular to the proximal-to-distal transect) were projected into the transect lines (in red boxes in Figs. 5-8). The proportions of each facies association were calculated in each projected well, and mean facies-association proportions were calculated in each projected group of closely spaced wells. The proportions of gravel, sand and mud grain size classes in each projected well and projected group of wells were calculated from these facies-association proportions and the proportions of gravel, sand and mud assigned to each facies association (Table 3). The wells and groups of wells therefore provide estimates of facies-association proportions and grain-size proportions at specific downsystem distances in each sediment routing system transect. Facies-association proportions and associated grain-size proportions at other points in each transect were estimated by simple linear interpolation between neighbouring pairs of wells and groups of wells in the transect. Facies-association and grain-size volumes between wells were estimated by multiplying the along-strike (i.e. transect-perpendicular) volumetric increments between wells by the mean facies-association and grain-size proportions of the pair

of wells that bound each volumetric increment. The sum of these along-strike (i.e. transect-perpendicular) facies-association and grain-size volumetric increments for a particular transect is the facies-association and grain-size volumes in the corresponding sediment routing system.

Errors in this step may arise because the wells and groups of wells in each sediment routing system transect are not representative of along-strike thicknesses and facies-association distributions. These errors can be qualitatively assessed by comparing the mean facies-association and grain-size proportions for groups of wells projected into the transect with the facies-association and grain-size proportions of individual wells in the group. Errors are greater where facies-associations pinch out laterally along-strike, for example because the facies associations occur in channelised bodies.

3.2.7 Step 7: Conversion of Grain-Size Volumes to Sediment Masses

Compacted grain-size volumes along each proximal-to-distal transect, as described in step 6 above and located in Figures 5-8 (in red boxes), are converted to sediment masses using bulk-density values derived from density logs in the studied wells (Fig. 4). We assign gravel conglomerates and sandstones a bulk density of 2400 kgm^{-3}, and mudstones a bulk density of 2500 kgm^{-3} (Okwara et al., 2023). These values include the effects of compaction and cementation, with cements generally considered to have been internally derived (e.g. Bjørlykke et al., 1992; Giles et al., 1992). Coal, which is generated biogenically *in situ* (e.g. Budding and Inglin, 1981; Livera, 1989), is excluded from our calculations of sediment mass.

3.2.8 Step 8: Calculation of Downsystem Extraction of Sediment Mass, Sediment Budgets, and Net-Depositional Mass Fluxes

In step 7, we calculated the sediment mass of each sediment routing system (as located in red boxes in Figs. 5-8). We then use a proximal-to-distal transect through each sediment routing system, combined with along-strike (i.e. transect-perpendicular) estimates of facies-association and grain-size volumes (step 6) and grain-size volume-to-mass conversions (step 7), to calculate the sequestration of sediment mass in the downsystem direction (i.e. from proximal to distal). The resulting downsystem extraction of sediment mass is normalised against the cumulative sediment mass in the sediment routing system volume (i.e., the parameter Chi, χ, of Strong et al. 2005), in order to provide a framework for comparison between the sediment routing systems (Strong et al. 2005; Paola and Martin, 2012). Within this framework, we compare two parameters from upsystem to downsystem.

First, we consider the proportion of gravel, sand, and mud grain-size classes in the sediment volume deposited by the sediment routing system in the proximal-to-distal transect. This parameter has been previously demonstrated to be independent of spatial variations in accommodation space (Strong et al., 2005; Duller et al., 2010; Whittaker et al., 2011; Paola and Martin, 2012; Michael et al., 2013). Consequently, differences in this parameter between sediment routing systems and/or between stratigraphic intervals can be attributed to: (1) the grain-size distribution input to the system; (2) along-strike influx to or efflux from the system; and/or (3) the grain-size distribution of bypassed sediment output from the system (cf. Hampson et al., 2014). The second of these three mechanisms suggests that the sediment routing system is

not closed, consistent with deposition in a wave-dominated delta(s) or other shorelines with significant along-shore sediment transport by waves, tides and marine currents (e.g. Hampson et al., 2014). The third mechanism would suggest that the full downsystem extent of the system has not been mapped, as has recently been implied for the 'Brent Delta' sediment routing system(s) by the sediment mass balance analysis of Okwara et al. (2023).

Second, we characterise the downsystem change in percentage-thickness, as a function of sediment mass extracted, of coastal-plain, marginal-marine, and shallow-marine-to-shelf sandstones (as defined by facies associations; Table 3). This parameter describes the upsystem-to-downsystem position of the palaeoshoreline, relative to the mass fraction of sandstone, in each sediment routing system, and may thus provide insights into the role of along-shore sand transport by waves, tides and marine currents.

Okwara et al. (2023) estimated the mass of deposited sediment in the 'Brent Delta' sediment routing system(s) in the J22, J24, J26 and J32 genetic sequences (using the full extent of sediment volumes mapped in Figs. 5A, 6A, 7A, 8A), and the sediment mass supplied to the combined J22-J32 interval from the Shetland Platform, Norwegian Landmass and Mid-North Sea High source areas (using the BQART sediment load model and, for the Mid-North Sea High, independent geometrical reconstruction of eroded volumes). When combined with the estimated durations of the J22, J24, J26 and J32 genetic sequences, Okwara et al. (2023) used these two values of sediment mass to construct, respectively, a net-depositional sediment budget (Fig. 11A) and a source-area sediment budget. We

use this mass-balance framework to contextualise the downsystem changes in grain-size that we derive from our analysis, and to interpret sediment budgets for gravel, sand and mud fractions in the ‘Brent Delta’ sediment routing system(s). The estimated durations of the J22, J24, J26 and J32 genetic sequences are used to calculate net-depositional mass fluxes for gravel, sand and mud fractions over the extent of each proximal-to-distal transect.

3.2.9 Errors and Uncertainties

Sources of error and uncertainty in each of the eight steps in our methodology are discussed below. Okwara et al. (2023) used a Monte Carlo approach to characterise error and uncertainty in their
estimated net-depositional and source-area sediment budgets (e.g. Fig. 11A). We refer to their results below without repeating, or extending, their analysis.

Uncertainty in the definition of stratigraphic intervals (step 1) arises from the biostratigraphic data and sequence stratigraphic concepts that underpin correlation of stratigraphic intervals and their bounding surfaces (e.g. Figs. 3, 9, 10). This uncertainty is defined by different correlation scenarios. For example, incorporating a revised biostratigraphic framework in Norwegian quadrant 15 (as used in Kieft et al., 2011) modifies the correlation of the J32 genetic sequence in the southern part of the study area (Fig. 10C) relative to the previous interpretation of Mitchener et al. (1992), which in turn affects the mapped thickness and palaeogeography of this genetic sequence (Fig. 8).

The thicknesses and areal extents of the stratigraphic intervals (step 2; Figs. 5-8) and the formulation of an age model (step 3; Fig. 3) are both considered in the uncertainty analysis of the net-depositional sediment budget of Okwara et al. (2023). The age model contributes up to 73% of the variance in the net-depositional sediment budget of individual genetic sequences (figure 9D in Okwara et al., 2023), and uncertainty in it arises from the resolution of biostratigraphic data and the accuracy of absolute ages to which the biostratigraphic data are calibrated (e.g. Gradstein et al., 2012; Ogg et al., 2016). The thicknesses and areal extents of the stratigraphic intervals in combination contribute up to 39% of the variance in the net-depositional sediment budget of individual genetic sequences (figure 9C in Okwara et al., 2023); this variance depends on the distribution and representativeness of well and seismic data that constrain isopach maps of the stratigraphic intervals (Figs. 5-8).

Delineation of the sediment routing system(s) in each stratigraphic interval (step 4) depends on the type, distribution, and quality of data that underpin reconstructions of palaeogeography (Figs. 5-8; e.g. Mitchener et al., 1992; Fjellanger et al., 1996; Husmo et al., 2003) and provenance (e.g. Morton, 1985, 1992; Hamilton et al., 1987; Hurst and Morton, 1988; Mearns, 1992). Uncertainty is defined by different palaeogeographic scenarios, and is mitigated in our analysis by using a simple model of three sediment source areas in the J22 and J32 genetic sequences that are amalgamated in the J24 and J26 genetic sequences (Figs. 5-8).

Uncertainty in the facies-association scheme that we use as a proxy for grain-size distributions (step 5) arises from the quantity, quality and representativeness of core

data that constrain the definition of facies associations and their constituent grain-size-class proportions (Table 3). Although we use a relatively small length of core (Table 2) and small number of wells (Fig. 4) to construct the facies-association scheme, it is similar to that used in many previous sedimentological studies of the Brent Group (Budding and Inglin, 1981; Richards and Brown, 1986; Graue et al., 1987; Livera, 1989; Ryseth, 1989; Livera and Caline, 1990; Mitchener et al., 1992; Scott, 1992; Johannessen et al., 1995; Fjellanger et al., 1996; Muto and Steel, 1997; Løseth and Ryseth, 2003; Morris et al., 2003; Hampson et al., 2004). We also use a simple grain-size characterisation scheme, with only gravel, sand and mud classes, in our analysis to reduce uncertainty.

Uncertainty in calculating facies-association and grain-size volumes in the sediment routing system(s) (step 6) reflects the quantity, quality and distribution of well data that underpin characterisation of facies-association volumes (e.g. Figs. 4, 9, 10). This uncertainty could be reduced by incorporating additional well data that constrain the distribution and pinch-out relationships of facies associations, particularly those that have channelised and lenticular geometries, but only at the expense of the time required for analysis. Given the large uncertainties in other methodological steps, particularly steps 2 and 3 (figure 9E in Okwara et al., 2023), and absence of wells in large parts of the study area (Fig. 4), we consider that the well database is sufficient for indicative, first-order approximations.

Okwara et al. (2023) considered conversion of grain-size volumes to sediment masses (step 7) in their uncertainty analysis of the net-depositional sediment budget of the J22, J24, J26 and J32 genetic sequences (their figure 9). Such uncertainty

arises from the quality and representativeness of wireline-log data that constrain the bulk density of the facies associations (e.g. Fig. 9) and is small, contributing only 3% of the variance in the net-depositional sediment budget of the combined J22-J32 interval (figure 9E in Okwara et al., 2023).

Uncertainty in the calculation of downsystem extraction of sediment mass, sediment budgets, and net-depositional mass fluxes (step 8) is compounded from sources of uncertainty in steps 1-7 of the methodology. In similar studies of ancient sediment routing systems, such compounded errors can result in halving or doubling of net-depositional mass flux estimates (e.g. Galloway, 2001; Hampson et al., 2014).

4. Results and Analysis

4.1. Grain-Size Fractions of the Total Sediment Mass

Our estimates of the gravel, sand and mud grain-size fractions of the total sediment mass in the J22, J24, J26 and J32 genetic sequences, derived using the methodology described above, are shown in Figure 11B. The estimates are for the areas defined by the red boxes in isopach maps and palaeogeographic reconstructions of each genetic sequence (Figs. 5-8). Genetic sequences J22 and J32 are subdivided into the deposits of three sediment routing systems (i.e. three red boxes in Figs. 5, 8), each with a distinct source area, whereas genetic sequences J24 and J26 are treated as the deposits of a single, composite sediment routing system (i.e. one red box in Figs. 6, 7). Consequently, a smaller proportion of the J24 and J26 deposits is sampled (i.e. cumulative area of three red boxes in Figs. 5, 8) than of the J24 and J26 deposits (i.e. area of one red box in Figs. 6, 7).

Similar grain-size fractions occur in all genetic sequences, with gravel, sand and mud constituting 0.7-2.1%, 45-62% and 38-54% of the total sediment mass, respectively (Fig. 11B). Given the large uncertainty in net-depositional sediment budget (Fig. 11A), it appears that the grain-size fractions supplied to the 'Brent Delta' sediment routing system(s) remained broadly similar throughout its deposition. The mean grain-size fractions of the total sediment mass for the J22, J24, J26 and J32 genetic sequences in combination are 1.0% gravel, 55% sand and 44% mud.

4.2. Downsystem Changes in Gravel, Sand and Mud Fractions

For each of the sediment routing systems in the J22, J24, J26 and J32 genetic sequences (defined by red boxes in Figs. 5-8), a proximal-to-distal transect was used to evaluate downsystem changes in grain-size fractions of the deposited sediment mass (Fig. 12A-C, 13A, 14A, 15A-C; Tables 4-7). These downsystem changes are expressed in terms of downsystem distance normalized to the sediment mass extracted by deposition (i.e., the parameter χ of Strong et al., 2005; Fig. 12A-C, 13A, 14A, 15A-C), with the total sediment mass for each proximal-to-distal transect defined for deposits in the area enclosing the transect (i.e. by a red box in Figs. 5-8). In addition to downsystem changes in gravel, sand and mud grain-size fractions (Fig. 12A-C, 13A, 14A, 15A-C), we also evaluate downsystem changes in the fraction of sand deposited in coastal-plain, marginal-marine and shallow-marine-to-shelf environments (Table 3), normalized to the sediment mass extracted by deposition (i.e., χ), along each proximal-to-distal transect (Fig. 12D-F, 13B, 14B, 15D-F). Distinguishing sand deposited in these three environments allows the effects of sampling channelised sandbodies, which are narrower than the spacing of wells in

the study dataset, to be identified, because channelised sandbodies occur in coastal-plain and marginal-marine environments (e.g. facies associations 1.1 and 2.2, Table 3) but not in shallow-marine-to-shelf environments (Table 3).

4.2.1 Genetic sequence J22

In genetic sequence J22, there are clear downsystem decreases in gravel and sand fractions in the deposits of sediment routing systems sourced from the Shetland Platform to the west (Figs. 5, 12A; Table 4) and from the Mid North Sea High to the south (Figs. 5, 12C; Table 4). Deposits of the sediment routing system sourced from the Norwegian Landmass to the east exhibit more variable upsystem-to-downsystem changes in gravel and sand fractions, including localised downsystem increases and downsystem decreases, such that there is no overall trend (Figs. 5, 12B; Table 4). These latter changes in sand fraction occur within shallow-marine-to-shelf environments, rather than in coastal-plain and marginal-marine environments that are channelised (Fig. 12E).

Downsystem decreases in gravel and sand fractions in deposits of the sediment routing systems sourced from the Shetland Platform and Mid North Sea High occur at $\chi = 0.5$ and $\chi = 0.6$, respectively (Fig. 12A, C), and are consistent with downsystem-fining due to sediment mass extraction by deposition (e.g. simple eastward pinchout of facies association 2.2, 3.1 and 3.2 sandstones in genetic sequence J22, Fig. 10A) (Strong et al., 2005; Paola and Martin, 2012). The more complex changes in sand fraction in deposits of the sediment routing system sourced from the Norwegian Landmass (Fig. 12B) are attributed to preferential accumulation of sand in Gilbert deltas located in antecedent half-graben depocentres

(Fig. 5A; Graue et al., 1987; Helland-Hansen et al., 1992; Muto and Steel, 1997). Sediment routing from the Norwegian Landmass to these Gilbert deltas was likely controlled by the three-dimensional topography associated with the antecedent half-graben, and is poorly approximated by the two-dimensional, proximal-to-distal transect used to characterise grain-size distribution (e.g. complex westward and eastward pinchouts of facies association 2.2 and 3.1 sandstones in genetic sequence J22, Fig. 10B).

4.2.2 Genetic sequence J24

In genetic sequence J24, downsystem changes in grain-size fractions are considered in the context of a single, composite sediment routing system sourced from the Shetland Platform, Mid North Sea High and Norwegian Landmass (Figs. 6, 13A; Table 5). The deposits of the composite sediment routing system exhibit a downsystem increase in gravel and sand fractions (from $\chi = 0$ to $\chi = 0.3$, Fig. 13A), followed by a decrease in gravel fraction and relatively uniform sand fraction (from $\chi = 0.3$ to $\chi = 0.9$, Fig. 13A) and a rapid downsystem decrease in gravel and sand fractions (from $\chi = 0.9$ to $\chi = 1.0$, Fig. 13A). The changes in sand fraction reflect an overall downsystem decrease in the proportion of coastal-plain and marginal-marine sand (from $\chi = 0$ to $\chi = 0.9$, Fig. 13B) and a corresponding overall downsystem increase in the proportion of shallow-marine-to-shelf sand (from $\chi = 0.1$ to $\chi = 0.9$, Fig. 13B), followed by a rapid downsystem decrease in the proportion of shallow-marine-to-shelf sand (from $\chi = 0.9$ to $\chi = 1.0$, Fig. 13B).

These changes in sand fraction are interpreted to reflect sand accumulation predominantly in coastal-plain and marginal-marine channels in upsystem locations

(from χ = 0 to χ = 0.3, Fig. 13; facies association 1.1 and 2.2 sandstones in genetic sequence J24, Fig. 10C), sand accumulation in a northward-prograding, wave-dominated shoreface and barrier-strandplain system (from χ = 0.3 to χ = 0.9, Fig. 13; facies association 2.2 and 3.2-3.4 sandstones in genetic sequence J24, Fig. 10), and palaeoseaward-decreasing sand content at the northward-progradational limit of the wave-dominated shoreface and barrier-strandplain system (from χ = 0.9 to χ = 1.0, Fig. 13; facies association 2.2 and 3.2-3.4 sandstones in genetic sequence J24, Fig. 10C) (Fig. 6; Graue et al., 1987; Helland-Hansen et al., 1992; Mitchener et al., 1992; Fjellanger et al., 1996; Hampson et al., 2004).

4.2.3 Genetic sequence J26

Downsystem changes in grain-size fractions in genetic sequence J26 are also considered in the context of a single, composite sediment routing system (Figs. 7, 14A; Table 6). The associated deposits exhibit relatively uniform gravel and sand fractions over much of their upsystem-to-downsystem extent (from χ = 0 to χ = 0.9, Fig. 14A), but with two localised maxima (at χ = 0.1 and χ = 0.9, Fig. 14A), followed by a rapid downsystem decrease in gravel and sand fractions (from χ = 0.9 to χ = 1.0, Fig. 14A).

In most upsystem-to-downsystem locations (from χ = 0 to χ = 0.9, Fig. 14B), the sand fraction is interpreted to reflect sampling of coastal-plain and marginal-marine channels (e.g. facies association 1.1 and 2.2 sandstones in genetic sequence J26, Fig. 10). At downsystem distances for which multiple wells are grouped (e.g. for which n ≥ 4, Figs. 14), there is sufficient sampling of channels and intervening interfluves that the mean value of sand fraction is constrained between 30 and 60%

(Fig. 14). At downsystem distances for which only one well is present (i.e. for which n = 1, Fig. 14), unrepresentatively high or low values of sand fraction are recorded (e.g. 90% in the localised peak at χ = 0.1, Fig. 14) depending on whether a channel or interfluve is sampled. The rapid downsystem decrease in gravel and sand fractions in downsystem locations (from χ = 0.9 to χ = 1.0, Fig. 14) is interpreted to reflect palaeoseaward-decreasing sand content at the northward-progradational limit of the wave-dominated shoreface and barrier-strandplain system (Fig. 7; facies association 3.2-3.4 sandstones in genetic sequence J26, Fig. 10C; Graue et al., 1987; Helland-Hansen et al., 1992; Mitchener et al., 1992; Fjellanger et al., 1996; Hampson et al., 2004).

4.2.4 Genetic sequence J32

Three distinct sediment routing systems are identified in genetic sequence J32 (Figs. 8, 15A-C; Table 7). Deposits of the sediment routing system sourced from the Shetland Platform to the west (Fig. 8) exhibits an overall downsystem decrease in sand fraction, but with a localised minimum between χ = 0.1 and χ = 0.3, in its deposits (Fig. 15A). Deposits of the sediment routing systems sourced from the Mid North Sea High to the south and from the Norwegian Landmass to the east (Fig. 8) both lack simple upsystem-to-downsystem trends in gravel and sand fractions (Figs. 8, 15B, C). For example, deposits of the sediment routing system sourced from the Norwegian Landmass High (Fig. 8) exhibit a downsystem increase in sand fraction (from χ = 0 to χ = 0.4, Fig. 15B) followed by a “noisy”, serrated decrease in sand fraction (from χ = 0.4 to χ = 1.0, Fig. 15B). The changes in sand fraction occur within shallow-marine-to-shelf environments, rather than in coastal-plain and marginal-marine environments, which are less abundant in the deposits of this sediment

routing system (Fig. 15E). The sand fraction of deposits of the sediment routing system sourced from the Mid North Sea (Fig. 8) increases downsystem overall, but this increase is subtle and masked by shorter-period changes (Fig. 15C). This overall trend is composed of a serrate downstream decrease in the sand fraction within coastal-plain and marginal-marine channels (Fig. 15F), combined with a downstream increase in the sand fraction within shallow-marine-to-shelf environments (from χ = 0.3 to χ = 1.0, Fig. 15F).

We tentatively attribute the upsystem-to-downsystem changes in gravel and sand fractions in deposits of the sediment routing systems sourced from the Shetland Platform and Norwegian Landmass (Fig. 15) to the initiation and growth of syn-depositional faults that are interpreted to have generated complex, three-dimensional patterns in sediment routing and accumulation (Fig. 8; Helland-Hansen et al., 1992; Mitchener et al., 1992; Fjellanger et al., 1996; Davies et al., 2000; McLeod et al., 2002; Hampson et al., 2004). These complex, three-dimensional patterns are poorly approximated by the two-dimensional, proximal-to-distal transects that we have used to characterise grain-size distribution (e.g. complex westward and eastward thickness variations and pinchouts of facies association 3.1-3.4 sandstones in genetic sequence J32, Fig. 10A, B). In the deposits of the sediment routing system sourced from the Mid North Sea High, upsystem-to-downsystem changes in the sand fraction are attributed to sparse sampling of coastal-plain and marginal-marine channels in well data ($n \leq 3$ at all downsystem distances, Fig. 15C, F; facies association 1.1 and 2.2 sandstones in genetic sequence J32, Fig. 10A) combined with sand accumulation in a series of retrogradationally stacked, southward-retreating, wave-dominated and weakly wave-influenced shoreface systems (from χ

= 0.3 to χ = 1.0, Fig. 15H facies association 2.2 and 3.1-3.4 sandstones in genetic sequence J32, Fig. 10A, B).

4.3. Estimated Net-Depositional Sediment Mass Fluxes

Net-depositional sediment mass fluxes in the 'Brent Delta' (corresponding to the depositional-sink sediment budgets of Okwara et al., 2023) were estimated for each genetic sequence using isopach maps (Figs. 5A, 6A, 7A, 8A) and estimated genetic-sequence durations (Okwara et al., 2023). We subdivide the net-depositional sediment mass fluxes for the J22 and J32 genetic sequences into contributions from three sediment routing systems (shown as three pie charts in Fig. 16A, D), consistent with our palaeogeographic reconstructions (Figs. 5B, 8B) and proximal-to-distal transects (Figs. 12, 15). The net-depositional sediment mass fluxes for the J24 and J26 genetic sequences are not subdivided (shown as a single pie chart in Fig. 16B, C), consistent with palaeogeographic reconstructions (Figs. 6B, 7B) and proximal-to-distal transects (Figs. 13, 14) for a single, composite sediment routing system. The gravel, sand and mud grain-size fractions of the net-depositional sediment mass fluxes are calculated following Step 6 of the method outlined above (Fig. 16).

4.3.1 Genetic sequence J22

Gravel net-depositional fluxes were low in the J22 genetic sequence: 0.002 Mt/yr, 0.002 Mt/yr and 0.001 Mt/yr in sediment routing systems sourced from the Shetland Platform, Norwegian Landmass and Mid North Sea High, respectively (Fig. 16A). The corresponding sand net-depositional fluxes were higher: 0.07 Mt/yr (Shetland Platform source area), 0.06 Mt/yr (Norwegian Landmass source area) and 0.02 Mt/yr

(Mid North Sea High source area), of similar or greater magnitude than mud net-depositional fluxes: 0.01 Mt/yr (Shetland Platform source area), 0.08 Mt/yr (Norwegian Landmass source area) and 0.01 Mt/yr (Mid North Sea High source area) (Fig. 16A).

4.3.2 Genetic sequence J24

Gravel, sand and mud net-depositional fluxes in the J24 genetic sequence were 0.02 Mt/yr, 2.0 Mt/yr and 1.2 Mt/yr, respectively, in the composite sediment routing system sourced from the Shetland Platform, Norwegian Landmass and Mid North Sea High (Fig. 16B).

4.3.3 Genetic sequence J26

In the J26 genetic sequence, gravel, sand and mud net-depositional fluxes in the composite sediment routing system were 0.05 Mt/yr, 1.6 Mt/yr and 2.0 Mt/yr, respectively (Fig. 16C).

4.3.4 Genetic sequence J32

Gravel net-depositional fluxes in the J32 genetic sequence were 0.004 Mt/yr (Shetland Platform source area), 0.006 Mt/yr (Norwegian Landmass source area) and 0.02 Mt/yr (Mid North Sea High source area) (Fig. 16D). The corresponding sand net-depositional fluxes were 0.4 Mt/yr (Shetland Platform source area), 0.6 Mt/yr (Norwegian Landmass source area) and 1.0 Mt/yr (Mid North Sea High source area) (Fig. 16D). Mud net-depositional fluxes were similar or smaller: 0.1 Mt/yr (Shetland Platform source area), 0.6 Mt/yr (Norwegian Landmass source area) and 0.8 Mt/yr (Mid North Sea High source area) (Fig. 16D).

The significant increase in net-depositional sediment mass fluxes between the J22 genetic sequence and the J24, J26 and J32 genetic sequences (Figs. 11A, 16) is attributed to uplift of the Mid-North Sea High source area (Underhill and Partington, 1993, 1994) and Norwegian Landmass source area (Gabrielsen et al., 2010; Ksienzyk et al., 2014; Medvedev and Hartz, 2015), potential catchment area expansion, and rift-related uplift of the Shetland Platform and Norwegian Landmass during deposition of the J32 genetic sequence (Helland-Hansen et al., 1992; Davies et al., 2000; Folkestad et al., 2014) (as synthesised in figure 14 of Okwara et al., 2023).

The gravel, sand and mud grain-size fractions of the net-depositional sediment mass fluxes are similar for all genetic sequences (Figs. 11B, 16), implying that there was not a significant change in the sediment grain-size composition supplied via sediment routing systems from the Shetland Platform, Norwegian Landmass and Mid North Sea High source areas. This may reflect spatio-temporal consistency of grain-size fractions generated in the source areas and/or buffering and mixing of sediment supply in source-area catchments (e.g. Castelltort and Van Den Driessche, 2003; Jerolmack and Paola, 2010; Straub et al., 2020). The small gravel grain-size fractions (Fig. 11B) and net-depositional fluxes (Fig. 16) imply that gravel may have been retained in source-area catchments. This inference is consistent with the rapid downsystem extraction of gravel into stratigraphy (i.e. for low values of χ) documented in other sediment routing systems (e.g. Michael et al., 2013). The relatively small mud grain-size fractions (Fig. 11B) and net-depositional fluxes (Fig. 16), which are similar to those for sand, are consistent with the interpretation that

mud was preferentially bypassed into more distal locations, beyond the depositional limit of the ‘Brent Delta’ (Okwara et al., 2023). The similarity in grain-size fractions of the net-depositional sediment mass fluxes in each genetic sequence (Figs. 11B, 16) implies either that: (1) the relative proportions of sediment supplied are insensitive to increases in catchment erosion rates, as required to account for the increase in sediment flux J22; or (2) the excess of a particular grain-size fraction, most likely mud, is preferentially bypassed downsystem.

4.4. Comparison to Source-Area and Depositional-Sink Sediment Budgets

We use the source-area sediment budgets, depositional-sink sediment budgets, and estimated durations of genetic sequences presented in Okwara et al. (2023) to construct sediment mass fluxes for the ‘Brent Delta’ sediment routing systems (Fig. 16). Okwara et al. (2023) used the BQART sediment load model (Syvitski and Milliman, 2007) to estimate source-area sediment budgets that are time-invariant over the duration of the J22, J24, J26 and J32 genetic sequences: 3.7 Mt/yr, 8.5 Mt/yr and 5.4 Mt/yr from the Shetland Platform, Mid North Sea High and Norwegian Landmass source areas, respectively (shown as black arrows from each source area in Fig. 16). Depositional-sink sediment budgets (Okwara et al., 2023) correspond to the net-depositional sediment mass fluxes described above (shown as pie charts in Fig. 16). There is a large discrepancy between the source-area sediment budgets and net-depositional sediment budgets for the ‘Brent Delta’ sediment routing systems, with the former being almost one order-of-magnitude larger than the latter (Okwara et al., 2023). This discrepancy implies large sediment bypass rates to the Faroe-Shetland Basin and/or western Møre Basin (13.3-17.2 Mt/yr for different

genetic sequences; shown as black arrows directed north out of the study area in Fig. 16).

5. Discussion

Paola and Martin (2012) argued that simple models of downsystem grain-size fining in a mass-balance framework can provide a useful reference for interpretation of complex, real-world systems that deviate from the simple reference state. Models of closed sediment routing systems (i.e. with no sediment mass transfer to or from neighbouring systems) indicate that grain size fines downsystem, when normalised by the total sediment mass, due to sediment mass extraction by deposition (Strong et al., 2005; Paola and Martin, 2012). As described above, the 'Brent Delta' sediment routing systems do not each exhibit a simple downsystem-fining trend in grain size (Figs. 12A-C, 13A, 14A, 15A-C), and thus differ from reference models. We discuss below: (1) the reasons for the deviation of the 'Brent Delta' sediment routing systems from the simple reference models; (2) how the deviation from simple reference models can potentially account for the apparent discrepancy between source-area and depositional-sink sediment budgets (Okwara et al., 2023); and (3) the broader implications for analysis of sediment routing systems.

5.1. Why do the 'Brent Delta' Deposits not Exhibit a Simple Downsystem-Fining Trend in Grain Size?

Although some of the sediment routing systems that we delineate in the 'Brent Delta' deposits (illustrated as transect lines in Figs. 5-8, 12A-C, 13A, 14A, 15A-C) exhibit a relatively simple downsystem-fining trend in grain size (Fig. 12A, C), most show

more complex upsystem-to-downsystem grain-size patterns (Figs. 12B, 13A, 14A, 15A-C). We identify three reasons, summarised below, for these complex patterns.

First, locally variable, “noisy” sand fractions in upsystem locations are attributed to sampling of laterally discontinuous, channelised sandbodies in coastal-plain and marginal-marine environments (facies associations 1.1 and 2.2, Table 3) by sparse, relatively widely spaced wells (from $\chi = 0$ to $\chi = 0.3$ in Fig. 13; from $\chi = 0$ to $\chi = 0.9$in Fig. 14; from $\chi = 0$ to $\chi = 1.0$ in Fig. 15C, F) (Fig. 17). Such local variations may be mitigated by increasing the number of wells, where sufficient well data are available, and thus sampling more representatively the channelised sandbodies and their intervening interfluves.

Second, locally variable sand fractions in non-channelised, marginal-marine and shallow-marine-to-shelf environments (facies associations 2.2 and 3.1-3.4, Table 3) in genetic sequences J22 and J32 are attributed to infilling of three-dimensional, rift-related, underfilled antecedent or syn-depositional topography (from $\chi = 0$ to $\chi = 1.0$ in Figs. 12B, E, 15A-B, D-E). Sediment routing and accumulation in the three-dimensional topography is sparsely sampled by the two-dimensional, proximal-to-distal transect lines in Figures 5, 8, which results in pronounced local minima and maxima in sand fraction. The resulting upsystem-to-downsystem patterns in gravel, sand and mud fractions are consistent with established interpretations of laterally stacked Gilbert deltas in antecedent half-graben depocentres in genetic sequence J22 (Fig. 5A; Graue et al., 1987; Helland-Hansen et al., 1992; Muto and Steel, 1997) and of shoreface sandstones in growing, underfilled half-graben depocentres in genetic sequence J32 (Fig. 8A; Helland-Hansen et al., 1992; Mitchener et al., 1992;

Fjellanger et al., 1996; Davies et al., 2000; McLeod et al., 2002; Hampson et al., 2004).

Third, downsystem-increasing or relatively uniform sand fractions in non-channelised, wave-dominated shallow-marine-to-shelf environments (facies associations 2.2 and 3.2-3.4, Table 3) are attributed to prograding or retrograding shoreface and barrier-strandplain systems that are not restricted to underfilled antecedent or syn-depositional depocentres (from $\chi = 0.3$ to $\chi = 0.9$ in Fig. 13; from $\chi = 0.3$ to $\chi = 1.0$ in Fig. 15C, F) (Fig. 17). The progradational limit of such wave-dominated shoreface and barrier-strandplain systems is marked by an abrupt downsystem decrease in sand fraction (from $\chi = 0.9$ to $\chi = 1.0$ in Fig. 13; from $\chi = 0.9$ to $\chi = 1.0$ in Fig. 14) (Fig. 17). These upsystem-to-downsystem patterns in grain-size fractions are consistent with established interpretations of wave-dominated, shoreface and barrier-strandplain deposits in genetic sequences J24, J26 and J32 (Fig. 6A, 7A, 8A; Graue et al., 1987; Helland-Hansen et al., 1992; Mitchener et al., 1992; Fjellanger et al., 1996; Hampson et al., 2004). Such wave-dominated shoreface and barrier-strandplain deposits are associated with nearshore retention of sand by shoaling fairweather waves (i.e. the ‘littoral energy fence’ of Swift and Thorne, 1991) and significant shoreline-parallel sediment transport, for example in response to oblique wave approach (e.g. Komar, 1976), as noted in previous interpretations of wave-dominated shoreface, strandplain and barrier island deposits in the ‘Brent Delta’ (Fig. 17; e.g. Mearns, 1992; Morton, 1992; Scott, 1992; Løseth and Ryseth, 2003; Went et al., 2013).

For each of these three reasons, spatial facies partitioning obscures downsystem-fining trends, particularly in the point-based observational data provided by wells. Incorporating additional wells may mitigate these effects to an extent, provided that they sample representatively the underlying facies distributions. However, spatial facies partitioning produced by processes that systematically redistribute sediment (e.g. waves and tides in shoreface-shelf settings) are still likely to distort simple downsystem-fining trends. Accounting for these processes requires mapping potentially complex sediment routing and dispersal patterns, and integrating these patterns across all grain-size fractions. In the 'Brent Delta' sediment routing systems, this approach would require adding the bypassed sediment mass to those characterised herein (Figs. 12-15). If such careful analysis of sediment routing and grain-size fractionation were carried out, sediment mass balance theory predicts that downstream extraction of sediment in χ space should recover the same simple downsystem-fining trend documented in physical experiments (e.g. Strong et al., 2005; Paola and Martin, 2012).

5.2. Can Downsystem Changes in Grain-Size Fractions Constrain the Budget of Bypassed Sediment Mass?

Source-area sediment budgets, which describe sediment influx from source-area catchments to the 'Brent Delta', are almost one order-of-magnitude larger than the net-depositional sediment budgets for the 'Brent Delta' sediment routing systems (Fig. 16; Okwara et al., 2023). This discrepancy implies that a large sediment mass is exported (or bypassed) northwards from the 'Brent Delta' sediment routing systems to the Faroe-Shetland Basin and/or western Møre Basin (13.3-17.2 Mt/yr for different genetic sequences; shown as black arrows directed north out of the study

area in Fig. 16). Below we consider the likely grain-size distributions released from the source-area catchments, how these grain-size distributions of the sediment supply compare to downsystem changes in grain-size fractions in the ‘Brent Delta’ deposits, and the implications for the volume and grain-size characteristics of sediment bypassed to the Faroe-Shetland Basin and/or western Møre Basin.

The proportion of gravel, sand and mud generated in, and exported from, catchments reflect their topography, exposed bedrock lithologies, climate, and sediment residence time (e.g. Whittaker et al., 2010; Allen et al., 2015; Watkins et al., 2020; Heins, 2023). In the source-area catchments that supplied sediment to the ‘Brent Delta’, the climate was sub-tropical and humid throughout the Middle Jurassic (Abbink et al., 2001; Sellwood and Valdes, 2006, 2008; Prokoph et al., 2008). Catchments on the Norwegian Landmass were composed of Precambrian gneisses and Caledonian metamorphic and granitic rocks (Morton et al., 2004), and had an estimated relief of 1-1.2 km during the Middle Jurassic (Gabrielsen et al., 2010; Medvedev and Hartz, 2015; Okwara et al., 2023). Such metamorphic bedrock lithologies fragment to give grain-size distributions with a relatively high proportion of sand and gravel (Palomares and Arribas, 1993; Allen et al., 2015; Fig. 17). Shetland Platform catchments were composed of Devonian, Carboniferous and Permo-Triassic sedimentary rocks (Morton et al., 2004), but their palaeotopography is poorly constrained (e.g. Okwara et al., 2023 used a value of 1.0 km in their application of the BQART sediment load model, assuming a similar uplift history to the Norwegian Landmass). Sedimentary bedrock lithologies fragment to give grain-size distributions with variable proportions of sand and gravel; relatively high proportions for reworked sandstones and relatively low proportions for reworked mudstones and limestones

(Arribas and Tortosa, 2003; Allen et al., 2015; Fig. 17). Sandstone-dominated Triassic and mudstone-dominated Lower Jurassic sedimentary rocks were eroded from catchments on the Mid North Sea High, which had a maximum relief of 0.3-0.5 km (Underhill and Partington, 1993; Okwara et al., 2023). Grain-size distributions with respectively high and low proportions of sand and gravel are likely to have been generated by the fragmentation and disaggregation of these sandstones and mudstones (cf. Arribas and Tortosa, 2003; Allen et al., 2015; Fig. 17). The grain-size distributions generated by fragmentation and weathering (Palomares and Arribas, 1993; Arribas and Tortosa, 2003; Allen et al., 2015) are modified by the duration and intensity of physical and chemical weathering during transport and storage (e.g. Heins and Kairo, 2007), although the resulting grain sizes retain a log-normal distribution (Allen et al., 2017).

In addition to the BQART model, Okwara et al. (2023) used a geometrical reconstruction of the Triassic and Lower Jurassic sedimentary rocks eroded from the Mid North Sea High to estimate source-area sediment budget. The geometrical reconstruction used median exhumed thicknesses of Triassic and Lower Jurassic strata of 0.4 km and 0.3 km, respectively (table 2 in Okwara et al., 2023). Based on lithological data from wells surrounding the Mid North Sea High (Husmo et al., 2003), we estimate that Triassic and Lower Jurassic strata had respective sandstone proportions of 50% and 20%, and mudstone proportions of 50% and 80%. If the exhumed sandstone was completely disaggregated to sand, and the exhumed mudstone to mud, then the resulting median estimate of sediment mass supplied by the catchment to the ‘Brent Delta’ was 25% sand and 75% mud. This value of sand mass content is less than half that of the estimated sand mass proportion in net-

depositional sediment budgets from the the Mid North Sea High (53-63% in genetic sequences J22 and J32; Fig. 16A, D), which implies that mud masses greater than the net-depositional sediment budgets were bypassed to the Faroe-Shetland Basin and/or western Møre Basin. Too few data are available for similar geometrical reconstructions and associated estimates of exhumed sediment mass proportions of the Shetland Platform and Norwegian Landmass source areas. However, as described above, the inferred fragmentation and weathering characteristics of exhumed bedrock in the Norwegian Landmass and Shetland Platform source areas implies that they probably released, respectively, more sand-rich and similarly sand-rich sediments to the 'Brent Delta' sediment routing systems (Fig. 17).

The downsystem-increasing or relatively uniform sand fractions in wave-dominated shoreface and barrier-strandplain deposits of genetic sequences J24 and J26 (from $\chi = 0.9$ to $\chi = 1.0$ in Fig. 13; from $\chi = 0.9$ to $\chi = 1.0$ in Fig. 14) are consistent with nearshore retention of sand within the 'littoral energy fence' (Swift and Thorne, 1991) and corresponding preferential offshore transport of mud. Thus, the sedimentological characteristics of the high sand fraction of the net-depositional sediment budgets (45-62% in genetic sequences J22-J32; Fig. 12B, 16) are also consistent with significant mud bypasss to the Faroe-Shetland Basin and/or western Møre Basin (Fig. 17). In order to balance the sediment mass supplied from source-area catchments with the net-depositional sediment budgets of the 'Brent Delta' deposits solely by trapping gravel and sand within the 'littoral energy fence', a sediment supply of approximately 0.02 Mt/yr of gravel, 1.3 Mt/yr of sand and 18.7 Mt/yr of mud is required, with 17.7 Mt/yr of this mud being exported to the Faroe-Shetland Basin and/or western Møre Basin. This is an end-member estimate, because net-import of

sand to wave-dominated shoreface and barrier-strandplain deposits via shoreline-parallel sediment transport, and/or net-export of mud by the same mechanism, can also contribute to balancing the source-area sediment budgets with the net-depositional sediment budgets. However, similarly large proportions of sediment bypass, associated with differential transport of sand and mud fractions, are noted in other source-to-sink studies (e.g. Angoche margin, Heins, 2023).

Although we cannot reach a definitive answer, a combination of: (1) export of sand-poor sediment from the Shetland Platform and Mid North Sea High source-area catchments with sedimentary bedrock; (2) retention of sand in wave-dominated shoreface and barrier-strandplain deposits by the 'littoral energy fence'; and (3) net-import of sand and/or next-export of mud by wave-generated longshore currents can account for much of the discrepancy between source-area sediment budgets and net-depositional sediment budgets of the 'Brent Delta' sediment routing systems (Fig. 17; Okwara et al., 2023). Furthermore, these mechanisms are consistent with available constraints from catchment bedrock lithology, sediment provenance and sedimentological facies analysis.

5.3. Implications for Future Analysis of Sediment Routing Systems in the Stratigraphic Record

Our results demonstrate that downsystem variations in grain size can be reconstructed in ancient sediment routing systems, even where grain-size data occur only in sparse and/or widely spaced subsurface wells. Reconstruction of these grain-size variations requires data that provide a sediment mass balance context: (1) a stratigraphic framework that can be applied over the full upsystem-to-downsystem

extent of the studied sediment routing system(s); (2) mapped sediment volumes for components of the stratigraphic framework; (3) provenance data that constrain sediment routing within the mapped sediment volumes; (4) a facies scheme appropriate for available data and in which facies have a distinct grain-size distribution; and (5) density data to convert sediment volumes to sediment masses. In addition, age data are required to integrate grain-size variations with sediment flux estimates, and thus to calculate sediment budgets.

The integration of downsystem variations in grain size (e.g. Reynolds, 2019) with sediment flux estimates (e.g. Brewer et al., 2020) provides a means to interpret sediment supply as a control on stratigraphic architecture at the resolution of the stratigraphic framework applied to the sediment routing system(s). Such interpretations are not straightforward, and need to be guided by facies models of the sediment routing system(s) that explicitly account for spatial facies partitioning. For example, the facies model of a wave-dominated delta ('Brent Delta') is required to interpret retention of sand in shoreface and barrier-strandplain facies by the 'littoral energy fence' (Swift and Thorne, 1991); this nearshore sand retention significantly modifies the simple downsystem-fining trend identified as a reference by Paola and Martin (2012) (Fig. 17). In addition, this facies model implies alongshore sediment transport that is consistent with heavy mineral provenance data (Morton, 1992). It also implies that the 'Brent Delta' sediment routing system(s) was not closed, and that the mapped sediment volumes do not account for the full sediment budget (cf. Angoche margin, Heins, 2023). Other deviations from the reference of a simple downsystem-fining grain-size trend are attributed to preferential trapping of sand and gravel by antecedent and growing, syn-depositional topography, and to

sparse, unrepresentative sampling of channelised sandbodies and their coeval sand-poor interfluves.

Despite potential ambiguity in interpretations, we consider that the analysis of downsystem grain-size variations in a sediment mass balance context provides insights that constrain sediment supply independent of the assumptions implicit in sequence stratigraphic models. In the context of the ‘Brent Delta’ sediment routing system(s), downsystem grain-size variations support the interpretation that large volumes of predominantly muddy sediment were bypassed beyond the down-dip limit of the wave-dominated delta front into the Faroes-Shetland Basin and Møre Basin (Figs. 2, 17). This interpretation is consistent with estimates of sediment supply derived from the BQART sediment-load model (Okwara et al., 2023). In contrast, sequence stratigraphic interpretations are inconsistent, and have proposed either the presence (e.g. Johannessen et al., 1995; Olsen and Steel, 1995) or absence of down-dip sediment bypass from the ‘Brent Delta’ (e.g. Went et al., 2013).

6. Conclusions

We reconstruct upsystem-to-downsystem variations in grain size in the sediment routing systems of the Middle Jurassic (Aalenian – Bathonian) Brent Group of the Northern North Sea in a sediment mass balance framework, in order to constrain sediment supply to the ‘Brent Delta’. Theory and experiments indicate that the preferential deposition of coarser grains during sediment transport generates a downsystem-fining grain-size trend that provides a reference to compare sediment routing systems, when the downsystem-fining trend is normalised with respect to

depositional sediment volume (i.e. accommodation space due to tectonic subsidence). Our analysis uses an integrated dataset of published age-constrained stratigraphic schemes, palaeogeographic reconstructions, regional isopach maps and provenance data to define the distribution of three sediment routing systems in four stratigraphic intervals. Within this context, facies-association proportions and distributions are estimated using representative core and wireline-log data. Facies associations are used as a textural proxy for gravel, sand and mud grain-size fractions, and thus enable reconstruction of upsystem-to-downsystem variations in grain size for each sediment routing system in each stratigraphic interval.

The Brent Group consists of four age-constrained genetic sequences. The oldest genetic sequence (J22) records the initial transverse progradation of basin-margin deltas sourced from the Shetland Platform to the west and Norwegian Landmass to the east, with subordinate progradation along the basin axis sourced from the Mid-North Sea High to the south. Subsequently, sediment routing systems sourced from the Shetland Platform, Norwegian Landmass and Mid-North Sea High combined to feed progradation and aggradation of a large wave-dominated delta along the basin axis (i.e. ‘Brent Delta’; genetic sequences J24 and J26). The youngest genetic sequence (J32) records overall shoreline retreat, during which the three sediment routing systems became geographically distinct.

Simple downsystem-fining trends in grain size, corresponding to the theoretical reference case, are rare in the Brent Group sediment routing systems for three reasons. (1) Locally variable, “noisy” sand fractions in upsystem locations of all sediment routing systems in all genetic sequences reflect sparse sampling of

laterally discontinuous, channelised sandbodies in coastal-plain and marginal-marine environments. (2) Locally variable sand fractions in non-channelised, marginal-marine and shallow-marine-to-shelf environments in transverse sediment routing systems in genetic sequences J22 and J32 are attributed to preferential trapping of sand in underfilled antecedent and syn-depositional, half-graben depocentres that are poorly represented in simple upsystem-to-downsystem transects. (3) Downsystem-increasing and relatively uniform sand fractions in non-channelised, wave-dominated shallow-marine-to-shelf environments in genetic sequences J24, J26 and J32 correspond to prograding or retrograding shoreface and barrier-strandplain systems, in which sand was retained near the shoreline by shoaling fairweather waves. By inference, wave-driven alongshore sediment transport was common in the 'Brent Delta' sediment routing system(s), which were not closed systems. The upsystem-to-downsystem variations in grain size described above are consistent with the prevailing, well-documented facies models and tectono-stratigraphic interpretations of the Brent Group, and demonstrate that spatial facies partitioning due to shallow-marine process regime is sufficient to distort the simple downsystem-fining trends predicted by sediment mass balance theory.

The deposits of the Brent Group sediment routing systems in each genetic sequence have a similar composition by mass: 0.7-2.1% gravel, 45-62% sand and 38-54% mud. These compositions are more sand-rich than those expected by fragmentation of bedrock lithologies in the Shetland Platform, Norwegian Landmass and Mid-North Sea High source areas, but are consistent with net input of sand to and/or net export of mud from the 'Brent Delta' sediment routing system(s) by alongshore sediment transport. Our reconstructed upsystem-to-downsystem variations in grain size thus

support the interpretation that large volumes of predominantly muddy sediment were bypassed beyond the down-dip limit of the 'Brent Delta', as implied by previous application of the BQART sediment-load model to the Brent Group sediment routing systems. Overall, our analysis illustrates the pragmatic application of downsystem-fining and sediment mass balance to interpreting the roles of sediment supply and sediment dispersal on stratigraphic architectures.

Acknowledgements

We thank Christopher Brewer, Christian Haug Eide, John Holbrook, Christopher Jackson, Howard Johnson and Oliver Jordan for constructive and encouraging discussions of this work, and the British Geological Survey (Nottingham, United Kingdom) and the Norwegian Petroleum Directorate (Stavanger, Norway) for permission to access subsurface core repositories and well data. Our research was supported by the Petroleum Technology Development Fund of Nigeria through a scholarship grant to ICO (project grant number: PTDF/ED/PHD/OIC/848/16).

Data availability statement

The data that underpin our study are publically available from the sources listed below: – core, offshore UK can be viewed at the National Geological Repository, British Geological Survey (https://www.bgs.ac.uk/geological-data/national-geological-repository/) – wireline logs, offshore UK from the UK National Data Repository, North Sea Transition Authority (https://ndr.nstauthority.co.uk) – core, offshore Norway can be viewed at the Geobank, Norwegian Petroleum Directorate (https://www.npd.no/en/facts/geology/geobank/) – wireline logs, offshore Norway from the Diskos Well Database, Norwegian Petroleum Directorate

(https://www.npd.no/en/diskos/wells/) – all other data are taken from publications, which are cited and listed in this paper.

Authors contribution

Ikenna Okwara: Conceptualization, Funding acquisition, Methodology, Investigation, Writing – original draft, Writing – review & editing.

Gary Hampson: Conceptualization, Data curation, Methodology, Supervision, Writing – review & editing.

Alexander Whittaker: Conceptualization, Supervision, Writing – review & editing.

Gareth Roberts: Conceptualization, Supervision, Writing – review & editing.

References

Abbink, O., Targarona, J., Brinkhuis, H. & Visscher, H. (2001). Late Jurassic to earliest Cretaceous palaeoclimatic evolution of the southern North Sea. *Global and Planetary Change*, *30*, 231-256. https://doi.org/10.1016/S0921-8181(01)00101-1

Allen, P.A. & Heller, P.L. (2011). Dispersal and preservation of tectonically generated alluvial gravels in sedimentary basins. *In:* C. Busby & A. Azor (Eds.), *Tectonics of sedimentary basins: recent advances*, Blackwell Publishing, Oxford, 111-130. https://doi.org/10.1002/9781444347166.ch6

Allen, P.A., Armitage, J.J., Carter, A., Duller, R.A., Michael, N.A., Sinclair, H.D., Whitchurch, A.L. & Whittaker, A.C. (2013). The Qs problem: sediment volumetric balance of proximal foreland basin systems. *Sedimentology*, *60*, 102-130. https://doi.org/10.1111/sed.12015

Allen, P.A., Armitage, J.J., Whittaker, A.C., Michael, N.A., Roda-Boluda, D. & D'Arcy, M. (2015). Fragmentation model of the grain size mix of sediment supplied to basins. *The Journal of Geology*, *123*, 405-427. https://doi.org/10.1086/683113

Allen, P.A., Michael, N.A., D'Arcy, M., Roda-Boluda, D.C., Whittaker, A.C., Duller, R.A. & Armitage, J.J. (2017). Fractionation of grain size in terrestrial sediment routing systems. *Basin Research*, *29*, 180-202. https://doi.org/10.1111/bre.12172

Armitage, J.J., Duller, R.A., Whittaker, A.C. & Allen, P.A. (2011). Transformation of tectonic and climatic signals from source to sedimentary archive. *Nature Geoscience*, *4*, 231-235. https://doi.org/10.1038/ngeo1087

Arribas, J. & Tortosa, A. (2003). Detrital modes in sedimenticlastic sands from low-order streams in the Iberian Range, Spain: the potential for sand generation by different sedimentary rocks. *Sedimentary Geology*, *159*, 275-303. https://doi.org/10.1016/S0037-0738(02)00332-9

Barnes, J.B. & Heins, W.A. (2009). Plio-Quaternary sediment budget between thrust belt erosion and foreland deposition in the central Andes, southern Bolivia. *Basin Research*, *21*, 91-109. https://doi.org/10.1111/j.1365-2117.2008.00372.x

Barton, P. & Wood, R. (1984). Tectonic evolution of the North Sea basin: crustal stretching and subsidence. *Geophysical Journal International*, *79*, 987-1022. https://doi.org/10.1111/j.1365-246X.1984.tb02880.x

Bhattacharya, J.P., Copeland, P., Lawton, T.F. & Holbrook, J. (2016). Estimation of source area, river paleo-discharge, paleoslope, and sediment budgets of linked deep-time depositional systems and implications for hydrocarbon

potential. *Earth-Science Reviews*, *153*, 77-110. https://doi.org/10.1016/j.earscirev.2015.10.013

Bjørlykke, K., Nedkvitne, T., Ramm, M. & Saigal, G.C. (1992). Diagenetic processes in the Brent Group (Middle Jurassic) reservoirs of the North Sea: an overview. *In:* A.C. Morton, R.S. Haszeldine, M.R. Giles & S. Brown (Eds.), *Geology of the Brent Group* Geological Society of London, Special Publication 61, 263-287. https://doi.org/10.1144/GSL.SP.1992.061.01.15

Brewer, C.J., Hampson, G.J., Whittaker, A.C., Roberts, G.G. & Watkins, S.E. (2020). Comparison of methods to estimate sediment flux in ancient sediment routing systems. *Earth-Science Reviews*, *207*, 103217. https://doi.org/10.1016/j.earscirev.2020.103217

Brommer, M.B., Weltje, G.J. & Trincardi, F. (2009). Reconstruction of sediment supply from mass accumulation rates in the northern Adriatic Basin (Italy) over the past 19,000 years. *Journal of Geophysical Research*, *114*, 1-15. https://doi.org/10.1029/2008JF000987

Budding, M.C. & Inglin, H.F. (1981). A reservoir geological model of the Brent Sands in southern Cormorant: Petroleum geology of the continental shelf of northwestern Europe. *In:* V. Illing, & G.D. Hobson (Eds.), *Petroleum Geology of the continental shelf of north-west Europe*, Institute of Petroleum, London, 326-334.

Burgess, P.M., & Steel, R.J. (2017). How to interpret, understand, and predict stratal geometries using stratal-control spaces and stratal-control-space trajectories. *Journal of Sedimentary Research*, *87*, 325-337. https://doi.org/10.2110/jsr.2017.19

Carvajal, C. & Steel, R.J. (2012). Source-to-sink sediment volumes within a tectono-stratigraphic model for a Laramide shelf-to-deep-water basin: methods and results. *In:* C. Busby & A. Azor (Eds.), *Tectonics of sedimentary basins: recent advances*, Blackwell Publishing, Oxford, 131-151. https://doi.org/10.1002/9781444347166.ch7

Castelltort, S. & Van Den Driessche, J. (2003). How plausible are high-frequency sediment supply-driven cycles in the stratigraphic record? *Sedimentary Geology*, *157*, p. 3-13. https://doi.org/10.1016/S0037-0738(03)00066-6

Catuneanu, O., Abreu, V., Bhattacharya, J.P., Blum, M.D., Dalrymple, R.W., Eriksson, P.G., Fielding, C.R., Fisher, W.L., Galloway, W.E., Gibling, M.R., Giles, K.A., Holbrook, J.M., Jordan, R., Kendall, C.G.St.C., Macurda, B., Martinsen, O.J., Miall, A.D., Neal, J.E., Nummedal, D., Pomar, L., Posamentier, H.W., Pratt, B.R., Sarg, J.F., Shanley, K.W., Steel, R.J., Strasser, A., Tucker, M.E., & Winker, C. (2009). Towards the standardization of sequence stratigraphy. *Earth-Science Reviews*, *92*, 1-33. https://doi.org/10.1016/j.earscirev.2008.10.003

Davies, S.J., Dawers, N.H., McLeod, A.E. & Underhill, J.R. (2000). The structural and sedimentological evolution of early syn-rift successions: the Middle Jurassic Tarbert Formation, North Sea. *Basin Research*, *12*, 343-365. https://doi.org/10.1111/j.1365-2117.2000.00136.x

Deegan, C.T. & Scull, B.J. (1977). *A standard lithostratigraphic nomenclature for the Central and Northern North Sea*. Report of the Institute of Geological Sciences, 77/25.

Duffy, O.B., Bell, R.E., Jackson, C.A-L., Gawthorpe, R.L., & Whipp, P.S. (2015). Fault growth and interactions in a multiphase rift fault network: Horda

Platform, Norwegian North Sea. *Journal of Structural Geology*, *80*, 99-119. https://doi.org/10.1016/j.jsg.2015.08.015

Duller, R.A., Whittaker, A.C., Fedele, J.J., Whitchurch, A.L., Springett, J., Smithells, R., Fordyce, S., & Allen, P.A. (2010). From grain size to tectonics. *Journal of Geophysical Research: Earth Surface*, *115*, F03022. https://doi.org/10.1029/2009JF001495

Færseth, R.B. (1996). Interaction of Permo-Triassic and Jurassic extensional fault-blocks during the development of the northern North Sea. *Journal of the Geological Society*, *153*, 931-944. https://doi.org/10.1144/gsjgs.153.6.0931

Fjellanger, E., Olsen, T.R. & Rubino, J.L. (1996). Sequence stratigraphy and palaeogeography of the Middle Jurassic Brent and Vestland deltaic systems, Northern North Sea. *Norsk Geologisk Tidsskrift*, *76*, 75-106.

Folkestad, A., Odinsen, T., Fossen, H. & Pearce, M.A. (2014). Tectonic influence on the Jurassic sedimentary architecture in the northern North Sea with focus on the Brent Group. *In:* A.W. Martinius, R. Ravnås, J.A. Howell, R.J. Steel & J.P. Wonham (Eds.), *From depositional systems to sedimentary successions on the Norwegian Continental Margin*, International Association of Sedimentologists, Special Publication 46, 389-416. https://doi.org/10.1002/9781118920435.ch14

Gabrielsen, R.H., Faleide, J.I., Pascal, C., Braathen, A., Nystuen, J.P., Etzelmuller, B., & O'Donnell, S. (2010). Latest Caledonian to Present tectonomorphological development of southern Norway. *Marine and Petroleum Geology*, *27*, 709-723. https://doi.org/10.1016/j.marpetgeo.2009.06.004

Galloway, W.E. (1989). Genetic stratigraphic sequences in basin analysis I: architecture and genesis of flooding-surface bounded depositional units. *American Association of Petroleum Geologists Bulletin*, *73*, 125-142. https://doi.org/10.1306/703C9AF5-1707-11D7-8645000102C1865D

Galloway, W.E. (2001). Cenozoic evolution of sediment accumulation in deltaic and shore-zone depositional systems, northern Gulf of Mexico Basin. *Marine and Petroleum Geology*, *18*, 1031-1040. https://doi.org/10.1016/S0264-8172(01)00045-9

Giles, M.R., Stevenson, S.V., Martin, S.V., Cannon, S.J.C., Hamilton, P.J., Marshall, J.D. & Samways, G.M. (1992). The reservoir properties and diagenesis of the Brent Group: a regional perspective. *In:* A.C. Morton, R.S. Haszeldine, M.R. Giles & S. Brown (Eds.), *Geology of the Brent Group* Geological Society of London, Special Publication 61, 289-327. https://doi.org/10.1144/GSL.SP.1992.061.01.16

Gradstein, F.M., Ogg, J.G., Schmitz, M.D. & Ogg, G.M. (Eds.) (2012). *The Geologic Time Scale 2012*. Elsevier.

Graue, E., Helland-Hansen, W., Johnsen, J., Lømo, L., Nøttvedt, A., Rønning, K., Ryseth, A. & Steel, R. (1987). Advance and retreat of Brent delta system, Norwegian North Sea. *In:* J. Brooks, & K. Glennie (Eds.), *Petroleum Geology of North West Europe, Volume 2*, Graham and Trotman, London, 915-937.

Hamilton, P.J., Fallick, A.E., Macintyre, R.M. & Elliot, S. (1987). Isotopic tracing of the provenance and diagenesis of Lower Brent Group sands, North Sea. *In:* J. Brooks, & K. Glennie (Eds.), *Petroleum Geology of North West Europe, Volume 2*, Graham and Trotman, London, 939-949.

Hampson, G.J. (2016). Towards a sequence stratigraphic solution set for autogenic processes and allogenic controls: Upper Cretaceous strata, Book Cliffs, Utah, USA. *Journal of the Geological Society*, *173*, 817-836. https://doi.org/10.1144/jgs2015-136

Hampson, G.J., Sixsmith, P.J. & Johnson, H.D. (2004). A sedimentological approach to refining reservoir architecture in a mature hydrocarbon province: the Brent Province, UK North Sea. *Marine and Petroleum Geology*, *21*, 457-484. https://doi.org/10.1016/S0264-8172(03)00094-1

Hampson, G.J., Duller, R.A., Petter, A.L., Robinson, R.A.J. & Allen, P.A. (2014) Mass-balance constraints on stratigraphic interpretation of linked alluvial-coastal-shelfal deposits: example from Cretaceous Western Interior Basin, Utah and Colorado, USA. *Journal of Sedimentary Research*, *84*, 935-960. https://doi.org/10.2110/jsr.2014.78

Haq, B.U. (2018). Jurassic sea-level variations: a reappraisal. *GSA Today*, *28*, 4-10. https://doi: 10.1130/GSATG359A.1

Heins, W.A. (2023). Honest bookkeeping for source-to-sink sediment mass-balance analysis with examples from the Angoche margin of Mozambique and the Corsica trough of France. *Marine and Petroleum Geology*, *153*, 106265. https://doi.org/10.1016/j.marpetgeo.2023.106265

Heins, W.A. & Kairo, S. (2007). Predicting sand character with integrated genetic analysis. *In:* J. Arribas, S. Critelli & M.J. Johnsson (Eds.), *Sedimentary Provenance and Petrogenesis: Perspectives from Petrography and Geochemistry*, Geological Society of America, Special Paper 420, 345-379. https://doi.org/10.1130/2006.2420(20)

Helland-Hansen, W., Ashton, M., Lømo, L., & Steel, R. (1992). Advance and retreat

of the Brent delta: recent contributions to the depositional model. *In:* A.C. Morton, R.S. Haszeldine, M.R. Giles & S. Brown (Eds.), *Geology of the Brent Group* Geological Society of London, Special Publication 61, 109-127. https://doi.org/10.1144/GSL.SP.1992.061.01.07

Heller, P.L., Burns, B.A., & Marzo, M. (1993). Stratigraphic solution sets for determining the roles of sediment supply, subsidence, and sea level on transgressions and regressions. *Geology*, **21**, 747-750. https://doi.org/10.1130/0091-7613(1993)021%3C0747:SSSFDT%3E2.3.CO;2

Holbrook, J. & Wanas, H. (2014). A fulcrum approach to assessing source-to-sink mass balance using channel paleohydrologic paramaters derivable from common fluvial data sets with an example from the Cretaceous of Egypt. *Journal of Sedimentary Research*, *84*, 349-372. https://doi.org/10.2110/jsr.2014.29

Hurst, A. & Morton, A.C. (1988). An application of heavy-mineral analysis to lithostratigraphy and reservoir modelling in the Oseberg Field, northern North Sea. *Marine and Petroleum Geology*, *5*, 157-169. https://doi.org/10.1016/0264-8172(88)90020-7

Husmo, T., Hamar, G.P., Høiland, O., Johannessen, E.P., Rømuld, A., Spencer, A.M. & Titterton, R. (2003). Lower and Middle Jurassic. *In:* D. Evans, C. Graham, A. Armour, & P. Bathurst (Eds.) *The Millenium Atlas: petroleum geology of the Central and Northern North Sea*, Geological Society of London, 129-155.

Jerolmack, D.J. & Paola, C. (2010). Shredding of environmental signals by sediment transport. *Geophysical Research Letters*, *37*, L19401. https://doi.org/10.1029/2010GL044638

Johannessen, E.R., Mjøs, R., Renshaw, D., Dalland, A. & Jacobsen, T. (1995). Northern limit of the “Brent delta” at the Tampen Spur - a sequence stratigraphic approach for sandstone prediction. *In:* R.J. Steel, V.L. Felt, E.P. Johannessen & C. Mathieu (Eds.), *Sequence stratigraphy on the Northwest European Margin*, Norwegian Petroleum Directorate, Special Publication 5, 213-256. https://doi.org/10.1016/S0928-8937(06)80070-6

Kieft, R.L., Jackson, C.A-L., Hampson, G.J. & Larsen, E. (2011). Sedimentology and sequence stratigraphy of the Hugin Formation, quadrant 15, Norwegian sector, South Viking Graben. *In:* B.A. Vining & S.C. Pickering (Eds.), *Petroleum geology: from mature basins to new frontiers - proceedings of the 7th Petroleum Geology Conference*, Geological Society of London, 157-176. https://doi.org/10.1144/0070157

Komar, P.D. 1976. *Beach Processes and Sedimentation*. Prentice Hall, New Jersey, 429p.

Ksienzyk, A.K., Dunkl, I., Jacobs, J., Fossen, H. & Kohlmann, F. (2014). From orogen to passive margin: constraints from fission track and (U-Th)/He analyses on Mesozoic uplift and fault reactivation in SW Norway. *In:* F. Corfu, D. Gasser & D.M. Chew (Eds.), *New perspectives on the Caledonides of Scandinavia and related areas*, Geological Society of London, Special Publication 390, 679-702. https://doi.org/10.1144/SP390.27

Livera, S.E. (1989). Facies associations and sand-body geometries in the Ness Formation of the Brent Group, Brent Field. *In:* M.K.G. Whateley & K.T. Pickering (Eds.), *Deltas: sites and traps for fossil fuels*, Geological Society of London, Special Publication 41, 269-286. https://doi.org/10.1144/GSL.SP.1989.041.01.19

Livera, S.E. & Caline, B. (1990). The sedimentology of the Brent Group in the Cormorant Block IV Oilfield. *Journal of Petroleum Geology*, *13*, 367-396. https://doi.org/10.1111/j.1747-5457.1990.tb00855.x

Løseth, T.M. & Ryseth, A. (2003). A depositional and sequence stratigraphic model for the Rannoch and Etive formations, Oseberg Field, northern North Sea. *Norwegian Journal of Geology*, *83*, 87-106.

Lyster, S.J., Whittaker, A.C., Allison, P.A., Lunt, D.J. & Farnsworth, A. (2020). Predicting sediment discharges and erosion rates in deep time - examples from the late Cretaceous North American continent. *Basin Research*, *32*, 1547-1573. https://doi.org/10.1111/bre.12442

McLeod, A.E., Dawers, N.H. & Underhill, J.R. (2000). The propogation and linkage of normal faults: insights from the Strathspey-Brent-Statfjord fault array, northern North Sea. *Basin Research*, *12*, 263-284. https://doi.org/10.1111/j.1365-2117.2000.00124.x

McLeod, A.E., Underhill, J.R., Davies, S.J. & Dawers, N.H. (2002). The influence of fault array evolution on synrift sedimentation patterns: controls on deposition in the Strathspey-Brent-Statfjord half graben, northern North Sea. *American Association of Petroleum Geologists Bulletin*, *86*, 1061-1093. https://doi.org/10.1306/61EEDC24-173E-11D7-8645000102C1865D

Mearns, E.W. (1992). Samarium-neodymium isotopic constraints on the provenance of the Brent Group. *In:* A.C. Morton, R.S. Haszeldine, M.R. Giles & S. Brown (Eds.), *Geology of the Brent Group* Geological Society of London, Special Publication 61, 213-225. https://doi.org/10.1144/GSL.SP.1992.061.01.12

Medvedev, S. & Hartz, E.H. (2015). Evolution of topography of post-Devonian Scandinavia: effects and rates of erosion. *Geomorphology*, *231*, 229-245. https://doi.org/10.1016/j.geomorph.2014.12.010

Michael, N.A., Whittaker, A.C. & Allen P.A. (2013). The functioning of sediment routing systems using a mass balance approach: example from the Eocene of the southern Pyrenees. *The Journal of Geology*, 121, 581-606. https://doi.org/10.1086/673176

Michael, N.A., Whittaker, A.C., Carter, A. & Allen P.A. (2014). Volumetric budget and grain-size fractionation of a geological sediment routing system: Eocene Escanilla Formation, South-Central Pyrenees. *Geological Society of America Bulletin*, 126, 585-599. https://doi.org/10.1130/B30954.1

Mitchener, B.C., Lawrence, D.A., Partington, M.A., Bowman, M.B.J. & Gluyas, J. (1992). Brent Group: sequence stratigraphy and regional implications. *In:* A.C. Morton, R.S. Haszeldine, M.R. Giles & S. Brown (Eds.), *Geology of the Brent Group* Geological Society of London, Special Publication 61, 45-80. https://doi.org/10.1144/GSL.SP.1992.061.01.05

Morris, J.E., Hampson, G.J. & Maxwell, G. (2003). Controls on facies architecture in the Brent Group, Strathspey Field, UK North Sea: implications for reservoir characterization. *Petroleum Geoscience*, *9*, 209-220. https://doi.org/10.1144/1354-079302-504

Morton, A.C. (1985). A new approach to provenance studies: electron microprobe analysis of detrital garnets from Middle Jurassic sandstones of the northern North Sea. *Sedimentology*, *32*, 553-566. https://doi.org/10.1111/j.1365-3091.1985.tb00470.x

Morton, A.C. (1992). Provenance of Brent Group sandstones: heavy mineral

constraints. *In:* A.C. Morton, R.S. Haszeldine, M.R. Giles & S. Brown (Eds.), *Geology of the Brent Group* Geological Society of London, Special Publication 61, 227-244. https://doi.org/10.1144/GSL.SP.1992.061.01.13

Morton, A.C., Hallsworth, C. & Chalton, B. (2004). Garnet compositions in Scottish and Norwegian basement terrains: a framework for interpretation of North Sea sandstone provenance. *Marine and Petroleum Geology*, *21*, 393-410. https://doi.org/10.1016/j.marpetgeo.2004.01.001

Muto, T. & Steel, R.J. (1997). The Middle Jurassic Oseberg Delta, northern North Sea: a sedimentological and sequence stratigraphic interpretation. *American Association of Petroleum Geologists Bulletin*, *81*, 1070-1086. https://doi.org/10.1306/522B49E7-1727-11D7-8645000102C1865D

Nyberg, B., Helland-Hansen, W., Gawthorpe, R.L., Sandbakken, P., Eide, C.H., Sømme, T., Hadler-Jacobsen, F. & Leiknes, S. (2018). Revisiting morphological relationships of modern source-to-sink segments as a first-order approach to scale ancient sedimentary systems. *Sedimentary Geology*, **373**, 111-133. https://doi.org/10.1016/j.sedgeo.2018.06.007

Ogg, J.G., Ogg, G.M. & Gradstein, F.M. (2016). *A concise geologic time scale*. Elsevier.

Okwara, I.C., Hampson, G.J., Whittaker, A.C., Roberts, G.G. & Ball, P.W. (2023). Source-to-sink mass-balance analysis of an ancient wave-influenced sediment routing system: Middle Jurassic Brent Delta, Northern North Sea, offshore UK and Norway. *Basin Research*, *35*, 1555-1589. https://doi.org/10.1111/bre.12765

Olsen, T.R. & Steel, R.J. 1995. Shoreface pinch-out style on the front of the Brent delta in the easterly Tampen Spur area. *In:* R.J. Steel, V.L. Felt, E.P.

Johannessen & C. Mathieu (Eds.), *Sequence stratigraphy on the Northwest European Margin*, Norwegian Petroleum Directorate, Special Publication 5, 273-289. https://doi.org/10.1016/S0928-8937(06)80072-X

Palomares, M., Arribas, J., Johnsson, M.J. & Basu, A. 1993. Modern stream sands from compound crystalline sources: composition and sand generation index. *In:* M.J. Johnsson & A. Basu (Eds.), *Processes Controlling the Composition of Clastic Sediment*, Geological Society of America, Special Paper 264, 313-320.

Paola, C. & Martin, J.M. (2012). Mass-balance effects in depositional systems. *Journal of Sedimentary Research*, *82*, 435-450. https://doi.org/10.2110/jsr.2012.38

Partington, M.A., Copestake, P., Mitchener, B.C. & Underhill, J.R. (1993). Biostratigraphic calibration of genetic stratigraphic sequences in the Jurassic–lowermost Cretaceous (Hettangian to Ryazanian) of the North Sea and adjacent areas. *In:* J.R. Parker (Ed.) *Petroleum geology of northwest Europe: proceedings of the 4th Petroleum Geology Conference*, Geological Society of London, 371-386. https://doi.org/10.1144/0040371

Phillips, T.B., Fazlikhani, H., Gawthorpe, R.L., Fossen, H., Jackson, C.A-L., Bell, R.E., Faleide, J.I. & Rotevatn, A. (2019). The influence of structural inheritance and multiphase extension on rift development, the Northern North Sea. *Tectonics*, *38*, 4099-4126. https://doi.org/10.1029/2019TC005756

Posamentier, H.W. & Vail, P.R. 1988. Eustatic controls on clastic deposition II - sequence and systems tract models. *In:* C.K. Wilgus, B.S. Hastings, C.G.S.C. Kendall, H.W. Posamentier, C.A. Ross, C.A. & J.C. Van Wagoner (Eds.), *Sea-level changes - an integrated approach*, Society for Sedimentary Geology (SEPM) Special Publication 42, 125-154.

Prokoph, A., Shields, G.A. & Veizer, J. (2008). Compilation and time-series analysis of a marine carbonate $\delta^{18}O$, $\delta^{13}C$, $^{87}Sr/^{86}Sr$ and $\delta^{34}S$ database through Earth history. *Earth-Science Reviews*, *87*, 113-133. https://doi.org/10.1016/j.earscirev.2007.12.003

Quirie, A.K., Schofield, N., Hartley, A., Hole, M.J., Archer, S.G., Underhill, J.R., Watson, D. & Holford, S.P. (2019). The Rattray Volcanics: Mid-Jurassic fissure volcanism in the UK Central North Sea. *Journal of the Geological Society*, *176*, 462-481. https://doi.org/10.1144/jgs2018-151

Rattey, R.P. & Hayward, A.B. (1993). Sequence stratigraphy of a failed rift system: the Middle Jurassic to Early Cretaceous basin evolution of the Central and Northern North Sea. *In:* J.R. Parker (Ed.) *Petroleum geology of northwest Europe: proceedings of the 4th Petroleum Geology Conference*, Geological Society of London, 215-249. https://doi.org/10.1144/0040215

Reynolds, A.D. 2019. “Grain-size bookkeeping,” a new aid for siliciclastic systems with examples from paralic environments. *Journal of Sedimentary Research*, *89*, 976-1016. https://doi.org/10.2110/jsr.2019.53

Richards, P.C. & Brown, S. (1986). Shoreface storm deposits in the Rannoch Formation (Middle Jurassic), North West Hutton oilfield. *Scottish Journal of Geology*, *22*, 367-375.

Romans, B.W., Castelltort, S., Covault, J.A., Fildani, A. & Walsh, J.P. (2016). Environmental signal propagation in sedimentary systems across timescales. *Earth-Science Reviews*, *153*, 7-29. https://doi.org/10.1016/j.earscirev.2015.07.012

Ryseth, A. (1989). Correlation of depositional patterns in the Ness Formation, Oseberg area. *In:* J.D. Collinson (Ed.) *Correlation in hydrocarbon exploration*,

Graham and Trotman, London, 313-326.

Scott, E.S. (1992). The palaeoenvironments and dynamics of the Rannoch-Etive nearshore and coastal succession, Brent Group, Northern North Sea. *In:* A.C. Morton, R.S. Haszeldine, M.R. Giles & S. Brown (Eds.), *Geology of the Brent Group* Geological Society of London, Special Publication 61, 129-147. https://doi.org/10.1144/GSL.SP.1992.061.01.08

Sellwood, B.W. & Valdes, P.J. (2006). Mesozoic climates: general circulation models and the rock record. *Sedimentary Geology*, *190*, 269-287. https://doi.org/10.1016/j.sedgeo.2006.05.013

Sellwood, B.W. & Valdes, P.J. (2008). Jurassic climates. *Proceedings of the Geologists Association*, *119*, 5-17. https://doi.org/10.1016/S0016-7878(59)80068-7

Snedden, J.W., Galloway, W.E., Milliken, K.T., Xu, J., Whiteaker, T. & Blum, M.D. (2018). Validation of empirical source-to-sink scaling relationships in a continental-scale system: The Gulf of Mexico basin Cenozoic record. *Geosphere*, **14**, 768-784. https://doi.org/10.1130/GES01452.1

Sneider, J.S., de Clarens, P. & Vail, P.R. (1995). Sequence stratigraphy of the Middle to Upper Jurassic, Viking Graben, North Sea. *In:* R.J. Steel, V.L. Felt, E.P. Johannessen & C. Mathieu (Eds.), *Sequence stratigraphy on the Northwest European Margin*, Norwegian Petroleum Directorate, Special Publication 5, 167-197. https://doi.org/10.1016/S0928-8937(06)80068-8

Steel, R.J. (1993). Triassic-Jurassic megasequence stratigraphy in the Northern North Sea: rift to post-rift evolution. *In:* J.R. Parker (Ed.) *Petroleum geology of northwest Europe: proceedings of the 4th Petroleum Geology Conference*, Geological Society of London, 299-315. https://doi.org/10.1144/0040299

Steel, R.J. & Ryseth, A. (1990). The Triassic – Early Jurassic succession in the northern North Sea: megasequence stratigraphy and intra-Triassic tectonics. *In:* R.P.F. Hardman & J. Brooks (Eds.), *Tectonic Events Responsible for Britain's Oil and Gas Reserves*, Geological Society of London, Special Publication 55, 139-168. https://doi.org/10.1144/GSL.SP.1990.055.01.07

Straub, K.M., Duller, R.A., Foreman, B.Z. & Hajek, E.A. (2020). Buffered, incomplete, and shredded: The challenges of reading an imperfect stratigraphic record. *Journal of Geophysical Research: Earth Surface*, *125*, e2019JF005079. https://doi.org/10.1029/2019JF005079

Strong, N., Sheets, B.A., Hickson, T.A. & Paola, C. (2005). A mass-balance framework for quantifying downstream changes in fluvial architecture. *In:* M.D. Blum, S.B. Marriott & S.F. Leclair (Eds.), *Fluvial Sedimentology VII*, International Association of Sedimentologists, Special Publication 35, 243–253. https://doi.org/10.1002/9781444304350.ch14

Swift, D.J.P. & Thorne, J.A. 1991. Sedimentation on continental margins, I: a general model for shelf sedimentation. *In:* D.J.P. Swift, G.F. Oertel, R.W. Tillman & J.A. Thorne (Eds.), *Shelf Sand and Sandstone Bodies: Geometry, Facies and Sequence Stratigraphy*, International Association of Sedimentologists, Special Publication 14, 3-31. https://doi.org/10.1002/9781444303933.ch1

Syvitski, J.P.M. & Milliman, J.D. (2007). Geology, geography, and humans battle for dominance over the delivery of fluvial sediment to the coastal ocean. *The Journal of Geology*, *115*, 1-19. https://doi.org/10.1086/509246

Sømme, T.O., Helland-Hansen, W., Martinsen, O.J. & Thurmond, J.B. (2009). Relationships between morphological and sedimentological parameters in source-to-sink systems: a basis for predicting semi-quantitative characteristics

in subsurface systems: *Basin Research*, *21*, 361-387. https://doi.org/10.1111/j.1365-2117.2009.00397.x

Torsvik, T.H., Carlos, D., Mosar, J., Cocks, L.R.M. & Malme, T. (2002). Global reconstructions and North Atlantic paleogeography 440 Ma to recent. *In:* E. Eide (Ed.) *BATLAS - Mid Norway plate reconstruction atlas with global and Atlantic perspectives*, Geological Survey of Norway, 18-19.

Underhill, J.R. & Partington, M.A. (1993). Jurassic thermal doming and deflation in the North Sea: implications of the sequence stratigraphic evidence. *In:* J.R. Parker (Ed.) *Petroleum geology of northwest Europe: proceedings of the 4th Petroleum Geology Conference*, Geological Society of London, 337-345. https://doi.org/10.1144/0040337

Underhill, J.R. & Partington, M.A. (1994). Use of genetic sequence stratigraphy in defining and determining a regional tectonic control on the “Mid Cimmerian Unconformity”: implications for North Sea Basin development and the global sea-level chart. *In:* P. Weimer & H.W. Posamentier (Eds.), *Siliciclastic sequence stratigraphy: recent developments and applications*, American Association of Petroleum Geologists, Memoir 58, 449-484.

Watkins, S.E., Whittaker, A.C., Bell, R.E., McNeill, L.C., Gawthorpe, R.L., Brooke, S.A. & Nixon, C.W. (2019). Are landscapes buffered to high-frequency climate change? A comparison of sediment fluxes and depositional volumes in the Corinth Rift, central Greece, over the past 130 ky. *Geological Society of America Bulletin*, **131**, 372-388. https://doi.org/10.1130/B31953.1

Watkins, S.E., Whittaker, A.C., Bell, R.E., Brooke, S.A., Ganti, V., Gawthorpe, R.L., McNeill, L.C. & Nixon, C.W. (2020). Straight from the source's mouth: controls on field-constrained sediment export across the entire active Corinth Rift,

central Greece. *Basin Research*, *32*, 1600-1625. https://doi.org/10.1111/bre.12444

Went, D.J., Hamilton, R.V., Platt, N.H. & Underhill, J.R. (2013). Role of forced regression in controlling Brent Group reservoir architecture and prospectivity in the northern North Sea. *Petroleum Geoscience*, *19*, 307-328. https://doi.org/10.1144/petgeo2013-028

Whitaker, M.F., Giles, M.R., & Cannon, S.J.C. (1992). Palynological review of the Brent Group, UK sector, North Sea. *In:* A.C. Morton, R.S. Haszeldine, M.R. Giles & S. Brown (Eds.), *Geology of the Brent Group* Geological Society of London, Special Publication 61, 169-202. https://doi.org/10.1144/GSL.SP.1992.061.01.10

Whittaker, A.C., Attal, M. & Allen, P.A. (2010). Characterising the origin, nature and fate of sediment exported from catchments perturbed by active tectonics. *Basin Research*, *22*, 809-828. https://doi.org/10.1111/j.1365-2117.2009.00447.x

Whittaker, A.C., Duller, R.A., Springett, J., Smithells, R.A., Whitchurch, A.L. & Allen, P.A. (2011). Decoding downstream trends in stratigraphic grain-size as a function of tectonic subsidence and sediment supply. *Bulletin of Geological Society of America*, *123*, 1363–1382. https://doi.org/10.1130/B30351.1

Zanella, E., & Coward, M.P. (2003). Structural framework. *In:* D. Evans, C. Graham, A. Armour, & P. Bathurst (Eds.) *The Millenium Atlas: petroleum geology of the Central and Northern North Sea*, Geological Society of London, 45-59.

Zhang, J., Covault, J., Pyrcz, M., Sharman, G., Carvajal, C. & Milliken, K. (2018). Quantifying sediment supply to continental margins: application to the

Paleogene Wilcox Group, Gulf of Mexico. *American Association of Petroleum Geologists Bulletin*, *102*, 1685-1702. https://doi.org/10.1306/01081817308

Zhang, J., Burgess, P.M., Granjeon, D. & Steel, R. (2019). Can sediment supply variations create sequences? Insights from stratigraphic forward modelling. *Basin Research*, *31*, 274-289. https://doi.org/10.1111/bre.12320

Ziegler, P.A. (1990). Tectonic and palaeogeographic development of the North Sea rift system. *In:* D.J. Blundell, & A.D. Gibbs (Eds.) *Tectonic evolution of the North Sea rifts*, Oxford University Press, 1-36.

Table 1. Wells in the study dataset (located in Fig. 4B), and previously published sequence stratigraphic frameworks (Fig. 3) that include interpretations of these wells.

Well (Fig. 4B)	Well name	Stratigraphic interpretation (Fig. 3)
1	34/2-4	after Fjellanger et al. (1996)
2	34/4-5	after Mitchener et al. (1992)
3	34/4-3	after Sneider et al. (1995)
4	211/13-6	Penguin Field; after Mitchener et al. (1992), Fjellanger et al. (1996)
5	211/19-6	Murchison Field; after Hampson et al. (2004)
6	211/18-21	Don Field; after Mitchener et al. (1992)
7	211/18-22	Don Field; after Fjellanger et al. (1996)
8	33/9-14	Statfjord Nord Field; after Fjellanger et al. (1996)
9	211/19-3	Murchison Field; after Hampson et al. (2004)
10	211/19-5	after Hampson et al. (2004)
11	211/19-1	Thistle Field; after Hampson et al. (2004)
12	211/18-19	Thistle Field; after Hampson et al. (2004)
13	211/16-6	Eider Field; after Fjellanger et al. (1996), Hampson et al. (2004)
14	210/20-2	after Hampson et al. (2004)
15	210/20-1	after Hampson et al. (2004)
16	210/25-2	Tern Field; after Hampson et al. (2004)
17	211/21-5	Cormorant North Field; after Hampson et al. (2004)
18	211/21-6	Cormorant North Field; after Hampson et al., 2004)
19	211/22-1	after Hampson et al. (2004)
20	211/22-2	after Fjellanger et al. (1996)
21	211/23-6	Dunlin South West; after Mitchener et al. (1992)
22	211/23-2	Dunlin South West; after Hampson et al. (2004)
23	211/24-5	after Hampson et al. (2004)
24	211/24-4	Statfjord Field; after Fjellanger et al. (1996)
25	33/9-3	Statfjord Field; after Fjellanger et al. (1996)
26	34/10-5	Gullfaks Field; after Mitchener et al. (1992)
27	34/8-1	Visund Field; after Fjellanger et al. (1996)
28	35/8-1	Vega Field; after Fjellanger et al. (1996)
29	35/8-3	after Fjellanger et al. (1996)
30	35/8-2	Vega Field; after Sneider et al. (1995)
31	35/11-2	after Sneider et al. (1995)
32	210/24-5	after Hampson et al. (2004)
33	211/26-2	Cormorant South Field; after Hampson et al. (2004)
34	211/27-3	North West Hutton Field; after Mitchener et al. (1992)
35	211/27-10	North West Hutton Field; after Hampson et al. (2004)
36	211/28-1	Hutton Field; after Fjellanger et al. (1996), Hampson et al. (2004)
37	211/28-5	after Fjellanger et al. (1996), Hampson et al. (2004)
38	211/29-3	Brent Field; after Fjellanger et al. (1996), Hampson et al. (2004)
39	211/29-2	Brent Field; after Hampson et al. (2004)
40	34/10-17	Gullfaks Sør Field; after Fjellanger et al. (1996)
41	34/10-23	Valemon Field; after Fjellanger et al. (1996)
42	2/5-3	Heather Field; after Hampson et al. (2004)
43	2/5-17	Broom Field; after Hampson et al. (2004)
44	3/1-1	after Hampson et al. (2004)
45	3/2-3	Lyell Field; after Hampson et al. (2004)
46	3/2-4	Lyell Field; after Hampson et al. (2004)
47	3/2-6	after Mitchener et al. (1992)
48	3/3-3	Ninian Field; after Mitchener et al. (1992), Hampson et al. (2004)
49	3/3-7	Ninian Field; after Hampson et al. (2004)
50	3/3-8	after Hampson et al. (2004)

51	3/4-1	Brent Field; after Hampson et al. (2004)
52	3/4-13	Strathspey Field; after Mitchener et al. (1992)
53	3/4-9	Strathspey Field; after Hampson et al. (2004)
54	3/4-12	Strathspey Field; after Hampson et al. (2004)
55	3/4-8	Alwyn North Field; after Hampson et al. (2004)
56	30/2-2	Huldra Field; after Fjellanger et al. (1996)
57	31/2-4	Troll Field; after Sneider et al. (1995)
58	31/2-3	Troll Field; after Sneider et al. (1995)
59	2/10-2	after Mitchener et al. (1992)
60	3/7-5	after Hampson et al. (2004)
61	3/8-6	Ninian Field; after Hampson et al. (2004)
62	3/12-2	after Mitchener et al. (1992)
63	3/8-10	Staffa Field; after Mitchener et al. (1992)
64	3/8-1	Ninian Field; after Mitchener et al. (1992)
65	3/9-4	Alwyn North Field; after Hampson et al. (2004)
66	3/9-2	Alwyn North Field; after Fjellanger et al. (1996)
67	3/10-1	after Hampson et al. (2004)
68	29/6-1	Martin Linge Field; after Fjellanger et al. (1996)
69	30/9-2	Oseberg Field; after Fjellanger et al. (1996)
70	30/6-8	after Fjellanger et al. (1996)
71	31/4-3	Brage Field; after Fjellanger et al. (1996)
72	31/6-8	Troll Field; after Fjellanger et al. (1996)
73	30/9-8	Oseberg Sør Field; after Fjellanger et al. (1996)
74	30/11-3	after Fjellanger et al. (1996)
75	25/2-7	after Fjellanger et al. (1996)
76	79/9-3	Bruce Field; after Mitchener et al. (1992)
77	9/13-12	Beryl Field; after Fjellanger et al. (1996)
78	24/6-1	after Fjellanger et al. (1996)
79	15/3-3	Gudrun Field; after Sneider et al. (1995), Kieft et al. (2011)
80	15/3-1	Gudrun Field; after Sneider et al. (1995), Kieft et al. (2011)
81	15/3-4	after Sneider et al. (1995), Kieft et al. (2011)
82	15/9-3	Sleipner Vest; after Sneider et al. (1995), Kieft et al. (2011)
83	15/9-1	Sleipner Vest; after Sneider et al. (1995), Kieft et al. (2011)
84	15/9-2	Sleipner Vest; after Sneider et al. (1995), Kieft et al. (2011)
85	15/9-7	Sleipner Vest; after Sneider et al. (1995), Kieft et al. (2011)

Table 2. Cored intervals studied for selected wells.

Well	Field name	Top core (m/ft)	Base core (m/ft)	Core recovery	Thickness (m)	Core-wireline shift (m/ft)
2/5-3	Heather	3350 m / 10992 ft	346 m / 11362 ft	100%	113	3.0 m / 10 ft
3/4a-12	Strathspey	2877 m / 9440 ft	3141 m / 10306 ft	100%	264	1.8 m / 6 ft
3/8b-10	Staffa	4052 m / 13294 ft	4176 m / 13701 ft	100%	124	3.0 m / 10 ft
9/9b-3	Bruce	3666 m / 12028 ft	4002 m / 13130 ft	88%	296	1.5 m / 5 ft
35/8-1	Vega	3523 m / 11557 ft	3710 m / 12171 ft	95%	187	1.2 m / 4 ft
210/20-2		2858 m / 9375 ft	2967 m / 9733 ft	100%	109	1.8 m / 6 ft
211/19-6	Murchison	3205 m / 10516 ft	3325 m / 10910 ft	100%	120	0.6 m / 2 ft
30/2-2	Huldra	3939 m / 12923 ft	4135 m / 13568 ft	100%	148	0 m / 0 ft
Total thickness					***1361***	

Table 3. Summary of interpreted facies associations, their sediment grain-size characteristics, and their wireline-log signatures (after Supplementary Material of Okwara et al., 2023).

Facies association	Lithostratigraphic distribution	Sedimentological description	Proportion of grain-size class	Wireline log response
1. Coastal plain				
1.1. Fluvial channel	Ness Fm.; Sleipner Fm.; Bruce 'C' Sands	Poorly to moderately sorted, fining-upward, fine- to coarse-grained sandstone (2-8 m thick). Pebble lag above erosional base. Cross-beds and asymmetrical ripples. Bioturbation absent to low in intensity.	gravel (g) - 5%; sand (s) - 90%; mud (m) - 5%	Low, upward-increasing gamma ray (20-40 API), moderate sonic (60-80 µs/ft), moderate to high density (2.4-2.6 g/cm^3), low neutron (2-25 p.u).
1.2. Floodplain	Ness Fm.; Sleipner Fm.	Mudstone (2-10 m thick) interbedded with very fine- to medium-grained sandstone. Plant root traces common. Bioturbation absent to moderate in intensity.	g - 0%; s - 20%; m - 80%	Variable, high gamma ray (60-90 API), high sonic (80-100 µs/ft), moderate to high density (2.35-2.7 g/cm^3), moderate to high neutron (15-50p.u.).
1.3. Swamp	Ness Fm.; Sleipner Fm.; Bruce B-C Coal	Coal and carbonaceous shale (<1 m thick). Bioturbation absent.	*In situ* biogenic accumulation	Low gamma ray (20-35 API), very high sonic (110-130 µs/ft), low density (1.6-1.8 g/cm^3), high neutron (50-60 p.u.).
2. Marginal marine				
2.1. Lagoon	Ness Fm.; Sleipner Fm.	Mudstone (1-4 m thick) with rare beds of very fine- to fine-grained sandstone. Parallel lamination, symmetrical and asymmetrical ripples. Rare hummocky cross-stratification. Sparse to moderate bioturbation intensity.	g - 0%; s - 20%; m - 80%	High gamma ray (70-80 API), moderate sonic (80-90 µs/ft), high density (2.6-2.65 g/cm^3), moderate to high neutron (30-45 p.u.).
2.2. Fluvio-tidal / estuarine channel and fan delta	Broom Fm.; Oseberg Fm.; Etive Fm.; Ness Fm.; Tarbert Fm.; Bruce 'B' Sands	Moderately to well-sorted, medium- to very coarse-grained sandstone (10-25 m thick) with sharp or erosional base. Cross-beds, asymmetrical ripples, mud drapes. Bioturbation is generally low to moderate in intensity.	g - 5%; s - 90%; m - 5%	Low to moderate, uniform to upward-increasing gamma ray (15-45 API), moderate to high sonic (60-95 µs/ft), moderate to high density (2.2-2.65 g/cm^3), low to moderate neutron (0.5-25 p.u.).
2.3. Bay-head and lagoonal delta	Ness Fm.; Sleipner Fm.	Very fine- to medium-grained, well to moderately sorted sandstone (3-7 m thick) usually interbedded with lagoon mudstone (FA 2.1). Symmetrical and asymmetrical ripples, low-angle cross-lamination, climbing asymmetrical ripples. Generally sparse to moderate bioturbation intensity.	g - 0%; s - 80%; m - 20%	Typically upward-decreasing gamma ray (20-70 API), moderate to high sonic (70-90 µs/ft), moderate density (2.3-2.55 g/cm^3), low to moderate neutron (6-28 p.u.).
1. Shallow marine to shelf				
3.1. Weakly wave-influenced (bioturbated) shoreface	Broom Fm.; Oseberg Fm.; Tarbert Fm.	Moderately to well-sorted, coarsening-upward, fine- to coarse-grained sandstone (10-20 m thick). Planar-parallel lamination and low-angle cross-lamination. Moderate to high bioturbation intensity in lower parts and low bioturbation intensity in upper parts of coarsening-upward units.	g - 0%; s - 100%; m - 0%	Moderate, upward-decreasing gamma ray (40-70 API), moderate sonic (75-85 µs/ft), moderate to high density (2.35-2.62 g/cm^3), moderate neutron (20-30 p.u.).
3.2. Wave-dominated upper shoreface and barrier bar	Etive Fm.; Hugin Fm.; Tarbert Fm.	Well-sorted, coarsening-upward, fine- to medium-grained sandstone (8-35 m thick). May appear structureless, but planar and trough cross-beds, asymmetrical ripples, planar-parallel lamination, low angle cross-lamination and dewatering structures occur. Absent to low bioturbation intensity.	g - 0%; s - 100%; m - 0%	Low, upward-decreasing gamma ray (10-35 API), moderate to high sonic (70-90 µs/ft), moderate density (2.2-2.6 g/cm^3), low to moderate neutron (3-30 p.u.).
3.3. Proximal lower shoreface	Rannoch Fm.; Hugin Fm.; Bruce 'A' Sands	Coarsening-upward succession of micaceous, well-sorted, fine- to lower medium-grained sandstone (5-25 m thick). Low-angle and hummocky cross-stratification, minor symmetrical and asymmetrical ripple cross-lamination. Bioturbation intensity is sparse to low.	g - 0%; s - 100%; m - 0%	Moderate, upward-increasing gamma ray (40-70 API), moderate sonic (70-85 µs/ft), variable density (2.3-2.7 g/cm^3), moderate neutron (20-36 p.u.).
3.4. Distal lower shoreface and offshore	lower Rannoch Fm.; Heather Fm.	Dominantly mudstone, may be interbedded with pinstripe laminae and thin beds of very fine- to fine-grained sandstone. Pyrite nodules and scattered shells occur. Bioturbation intensity is moderate to intense.	g - 0%; s - 0%; m - 100%	High gamma ray (55-120 API), moderate to high sonic (80-95 µs/ft), high density (2.5-2.65 g/cm^3), variable neutron porosity (12-40 p.u.).

Table 4. Calculated values of downsystem extraction of cumulative sediment mass normalised against the cumulative sediment mass in the sediment routing system volume (χ) for genetic sequence J22 (cf. Figs. 5, 10A-C, 12).

transverse transect for western basin margin, sourced from Shetland Platform (Fig. 12A, D)			
Wells at location	downsystem distance (km)	cumulative sediment mass extracted upsystem (x10^{12} kg)	Proportion of total sediment mass extracted upsystem (χ)
western boundary	0	0	0
210/24a-5, 2/5-17 (n=2)	16	8.70	0.03
2/5-3, 2/10a-2, 210/20-1, 210/20-2, 210/25-2, 211/26-2 (n=6)	29	87.7	0.27
3/1-1, 3/2-3, 211/16-6, 211/21-5, 211/21-6, 211/22-1 (n=6)	36	131	0.40
3/2-4, 3/2-6, 3/3-3, 3/7b-5, 3/8-6, 3/12-2, 211/22-2, 211/27-3, 211/27-10, 211/28-1 (n=10)	44	159	0.48
3/3-8, 3/3-7, 3/8-1, 3/8b-10, 211/13-6, 211/18-19, 211/18a-21, 211/18-22, 211/19-1, 211/23-2, 211/23-6, 211/28-5 (n=12)	57	217	0.66
3/4a-12, 3/4a-13, 3/4-1, 3/4-8, 3/4-9, 3/9-2, 3/9-4, 211/19-3, 211/19-5, 211/19-6, 211/24-2, 411/24-5, 211/29-2, 211/29-3 (n=14)	62	237	0.72
33/9-3, 33/9-14, 29/6-1, 3/10-1 (n=4)	77	295	0.89
34/10-5, 34/10-17, 34/4-3 (n=3) = eastern boundary	87	330	1.00

transverse transect for eastern basin margin, sourced from Norwegian Landmass (Fig. 12B, E)			
Wells at location	downsystem distance (km)	cumulative sediment mass extracted upsystem (x10^{12} kg)	Proportion of total sediment mass extracted upsystem (χ)
eastern boundary	0	0	0
31/6-8 (n=1)	39	64.2	0.12
31/2-3, 31/2-4, 35/8-3, 35/11-2 (n=4)	58	194	0.35
35/8-1, 35/8-2 (n=2)	60	208	0.38
31/4-3 (n=1)	76	293	0.53
30/6-8 (n=1)	85	334	0.61
30/9-2, 30/9-8 (n=2)	91	385	0.70
30/2-2, 34/2-4 (n=2)	107	496	0.90
34/8-1 (n=1)	110	509	0.93
34/10-23, 34/4-5 (n=2) = eastern boundary	119	550	1.00

axial transect for southern basin margin, sourced from Mid-North Sea High (Fig. 12C, F)			
Wells at location	downsystem distance (km)	cumulative sediment mass extracted upsystem (x10^{12} kg)	Proportion of total sediment mass extracted upsystem (χ)
southern boundary	0	0	0
24/6-1, 9/13-12st (n=2)	50	26.4	0.22

9/9b-3 (n=1)	74	72.2	0.60
25/2-7 (n=1)	89	97.4	0.81
30/11-3 (n=1) = northern boundary	101	121	1.00

Table 5. Calculated values of downsystem extraction of cumulative sediment mass normalised against the cumulative sediment mass in the sediment routing system volume (χ) for genetic sequence J24 (cf. Figs. 6, 10A-C, 13).

axial transect for southern basin margin, sourced from Shetland Platform, Norwegian Landmass and Mid-North Sea High (Fig. 13)			
Wells at location	downsystem distance (km)	cumulative sediment mass extracted upsystem (x10^{12} kg)	Proportion of total sediment mass extracted upsystem (χ)
southern boundary	0	0	0
24/6-1, 9/13-12st (n=2)	109	81.5	0.02
25/2-7 (n=1)	148	231	0.07
30/11-3 (n=1)	160	323	0.09
30/9-2, 30/9-8 (n=2)	197	639	0.18
29/6-1, 30/6-8, 31/4-3, 31/6-8 (n=4)	211	773	0.22
2/10a-2, 3/8-6, 3/8b-10, 3/7b-5 (n=4)	229	1050	0.30
3/2-6, 3/4-8, 3/8-1, 3/9-2, 3/9a-4, 3/10-1, 30/2-2, 31/2-3, 31/2-4 (n=9)	237	1200	0.34
2/5-17, 3/1-1, 3/2-3, 3/2-4, 3/3-3, 3/3-7, 3/3-8, 3/4a-12, 3/4a-13 (n=9)	246	1370	0.39
2/5-3, 3/4-1, 211/29-2, 34/10-23 (n=4)	256	1580	0.44
211/26-2, 211/27-3, 211/27-10, 211/28-1, 211/28-5, 211/29-3, 34/10-17 (n=7)	260	1690	0.48
210/24a-5, 211/21-5, 211/21-6, 211/22-2, 211/23-2, 211/23-6, 211/24-4, 211/24-5, 34/10-5, 35/11-2 (n=10)	277	2220	0.63
210/25-2, 211/22-1, 33/9-3, 35/8-2 (n=4)	289	2640	0.74
211/16-6, 211/18-19, 211/19-1, 211/19-3, 211/19-5, 34/8-1, 35/8-1, 35/8-2 (n=8)	301	3080	0.87
210/20-1, 210/20-2, 211/18a-21, 211/18-22, 211/19-6, 33/9-14 (n=6)	303	3180	0.90
211/13-6, 34/4-3, 34/4-5 (n=3)	312	3390	0.96
34/2-4 (n=1) = northern boundary	339	3550	1.00

Table 6. Calculated values of downsystem extraction of cumulative sediment mass normalised against the cumulative sediment mass in the sediment routing system volume (χ) for genetic sequence J26 (cf. Figs. 7, 10A-C, 14).

axial transect for southern basin margin, sourced from Shetland Platform, Norwegian Landmass and Mid-North Sea High (Fig. 14)			
Wells at location	downsystem distance (km)	cumulative sediment mass extracted upsystem (x10^{12} kg)	Proportion of total sediment mass extracted upsystem (χ)
southern boundary	0	0	0
24/6-1, 9/13-12st (n=2)	109	233	0.07
9/9b-3 (n=1)	133	437	0.13
25/2-7 (n=1)	148	617	0.19
30/11-3 (n=1)	160	750	0.23
30/9-2, 30/9-8 (n=2)	197	1190	0.36
29/6-1, 30/6-8, 31/4-3, 31/6-8 (n=4)	211	1370	0.42
2/10a-2, 3/8-6, 3/8b-10, 3/7b-5 (n=4)	229	1640	0.50
3/2-6, 3/4-8, 3/8-1, 3/9-2, 3/9a-4, 3/10-1, 30/2-2, 31/2-3, 31/2-4 (n=9)	237	1770	0.54
2/5-17, 3/1-1, 3/2-3, 3/2-4, 3/3-3, 3/3-7, 3/3-8, 3/4a-12, 3/4a-13 (n=9)	246	1960	0.60
2/5-3, 3/4-1, 211/29-2, 34/10-23 (n=4)	256	2160	0.66
211/26-2, 211/27-3, 211/27-10, 211/28-1, 211/28-5, 211/29-3, 34/10-17 (n=7)	260	2260	0.69
210/24a-5, 211/21-5, 211/21-6, 211/22-2, 211/23-2, 211/23-6, 211/24-4, 211/24-5, 34/10-5, 35/11-2 (n=10)	277	2640	0.80
210/25-2, 211/22-1, 33/9-3, 35/8-2 (n=4)	289	2850	0.87
211/16-6, 211/18-19, 211/19-1, 211/19-3, 211/19-5, 34/8-1, 35/8-1, 35/8-2 (n=8)	301	3030	0.92
210/20-1, 210/20-2, 211/18a-21, 211/18-22, 211/19-6, 33/9-14 (n=6)	303	3070	0.94
211/13-6, 34/4-3, 34/4-5 (n=3)	312	3170	0.96
34/2-4 (n=1) = northern boundary	339	3290	1.00

Table 7. Calculated values of downsystem extraction of cumulative sediment mass normalised against the cumulative sediment mass in the sediment routing system volume (χ) for genetic sequence J32 (cf. Figs. 8, 10A-C, 15).

transverse transect for western basin margin, sourced from Shetland Platform (Fig. 15A, D)			
Wells at location	downsystem distance (km)	cumulative sediment mass extracted upsystem (x10^{12} kg)	Proportion of total sediment mass extracted upsystem (χ)
western boundary	0	0	0
210/24a-5, 2/5-17 (n=2)	16	110	0.09
2/5-3, 2/10a-2, 210/20-1, 210/20-2, 210/25-2, 211/26-2 (n=6)	29	168	0.14
3/1-1, 3/2-3, 211/16-6, 211/21-5, 211/21-6, 211/22-1 (n=6)	36	196	0.17
3/2-4, 3/2-6, 3/3-3, 3/7b-5, 3/8-6, 3/12-2, 211/22-2, 211/27-3, 211/27-10, 211/28-1 (n=10)	44	241	0.20
3/3-8, 3/3-7, 3/8-1, 3/8b-10, 211/13-6, 211/18-19, 211/18a-21, 211/18-22, 211/19-1, 211/23-2, 211/23-6, 211/28-5 (n=12)	57	361	0.31
3/4a-12, 3/4a-13, 3/4-1, 3/4-8, 3/4-9, 3/9-2, 3/9-4, 211/19-3, 211/19-5, 211/19-6, 211/24-2, 411/24-5, 211/29-2, 211/29-3 (n=14)	62	448	0.38
33/9-3, 33/9-14, 29/6-1, 3/10-1 (n=4)	77	881	0.74
34/10-5, 34/10-17, 34/4-3 (n=3) = eastern boundary	87	1190	1.00

transverse transect for eastern basin margin, sourced from Norwegian Landmass (Fig. 15B, E)			
Wells at location	downsystem distance (km)	cumulative sediment mass extracted upsystem (x10^{12} kg)	Proportion of total sediment mass extracted upsystem (χ)
eastern boundary	0	0	0
31/6-8 (n=1)	39	98.3	0.04
31/2-3, 31/2-4, 35/8-3, 35/11-2 (n=4)	58	384	0.15
35/8-1, 35/8-2 (n=2)	60	414	0.16
31/4-3 (n=1)	76	794	0.30
30/6-8 (n=1)	85	1150	0.44
30/9-2, 30/9-8 (n=2)	91	1480	0.56
30/2-2, 34/2-4 (n=2)	107	2210	0.84
34/8-1 (n=1)	110	2340	0.89
34/10-23, 34/4-5 (n=2) = eastern boundary	119	2630	1.00

axial transect for southern basin margin, sourced from Mid-North Sea High (Fig. 15C, F)			
Wells at location	downsystem distance (km)	cumulative sediment mass extracted upsystem (x10^{12} kg)	Proportion of total sediment mass extracted upsystem (χ)
southern boundary	0	0	0
15/9-2, 15/9-3, 15/9-7 (n=3)	81	559	0.14

15/3-1, 15/3-3 (n=2)	130	1090	0.27
24/6-1, 9/13-12st (n=2)	198	2240	0.56
9/9b-3 (n=1)	222	2950	0.74
25/2-7 (n=1)	237	3490	0.88
30/11-3 (n=1) = northern boundary	249	3990	1.00

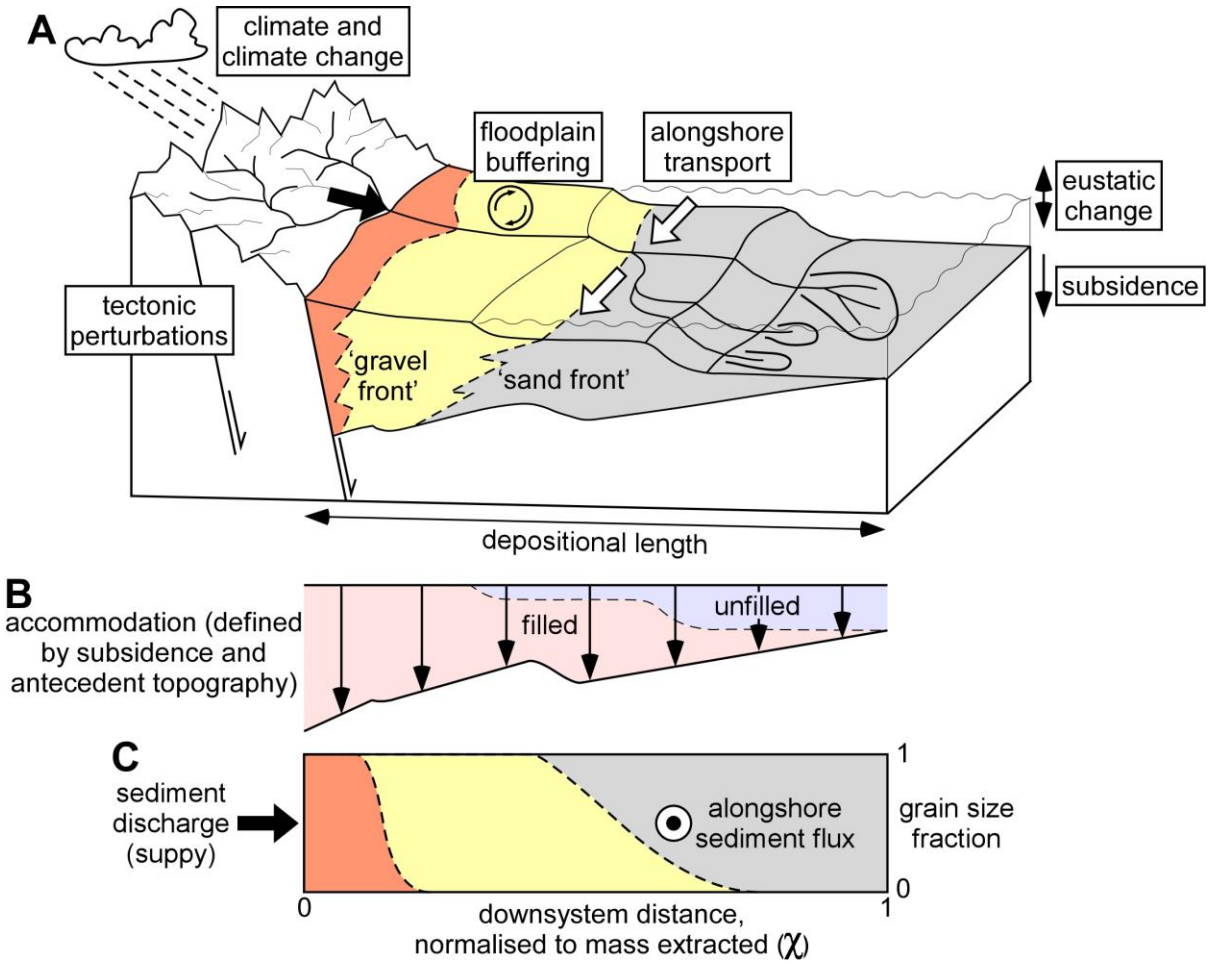

Figure 1. (**A**) Schematic illustration of a sediment routing system, which links sediment source areas to depositional sinks, and controls on its development (after Allen and Heller, 2011). These controls force the moving boundaries of the system (e.g. gravel front, sand front, shoreline) to migrate. Stratigraphy results from mass extraction (i.e. to deposition) from the surface sediment flux, and the depositional flux depends on (**B**) the spatial and temporal distribution of accommodation. (**C**) Sediment distribution in a mass balance framework, in which downsystem distance is transformed to the mass extraction domain; the downsystem coordinate χ shows the depositional mass extracted upsystem, normalised to the total sediment mass deposited in the sediment routing system from source to sink (e.g. Paola and Martin, 2012). The mass balance framework allows sediment routing systems of different scales and spatio-temporal accommodation-space distributions to be compared.

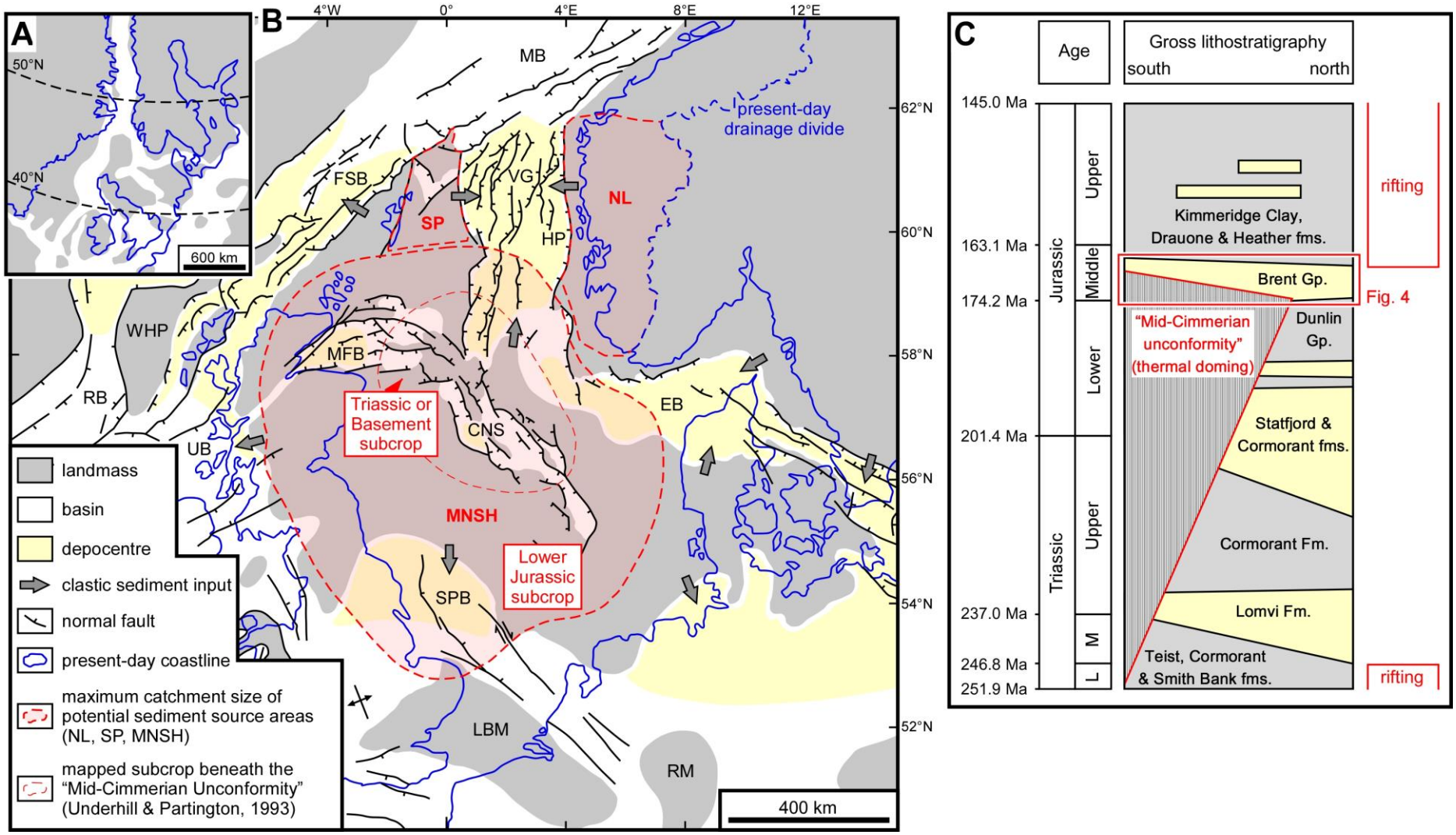
A
50°N
40°N
600 km
B
4°W
0°
4°E
8°E
12°E
62°N
60°N
58°N
56°N
54°N
52°N
MB
present-day drainage divide
FSB
VG
NL
SP
HP
WHP
MFB
RB
Triassic or Basement subcrop
CNS
EB
UB
MNSH
Lower Jurassic subcrop
SPB
LBM
RM
400 km
landmass
basin
depocentre
clastic sediment input
normal fault
present-day coastline
maximum catchment size of potential sediment source areas (NL, SP, MNSH)
mapped subcrop beneath the "Mid-Cimmerian Unconformity" (Underhill & Partington, 1993)
C
Age
Gross lithostratigraphy
south
north
145.0 Ma
163.1 Ma
174.2 Ma
201.4 Ma
237.0 Ma
246.8 Ma
251.9 Ma
Jurassic
Triassic
Upper
Middle
Lower
Upper
M
L
Kimmeridge Clay, Drauone & Heather fms.
Brent Gp.
"Mid-Cimmerian unconformity" (thermal doming)
Dunlin Gp.
Statfjord & Cormorant fms.
Cormorant Fm.
Lomvi Fm.
Teist, Cormorant & Smith Bank fms.
rifting
Fig. 4
rifting

Figure 2. (**A**) Unrestored Middle Jurassic palaeogeographic reconstruction of the North Sea (Ziegler, 1990; Torsvik et al., 2002). (**B**) Restored Middle Jurassic palaeogeographic reconstruction of the Northern North Sea showing palaeo-landmasses and basins (Ziegler, 1990). Note the extent of the proto-Viking Graben (VG) and sediment input into the basin from the Shetland Platform (SP), Norwegian Landmass (NL), and Mid-North Sea High (MNSH). Additional tectonic elements include the Central North Sea (CNS), Egersund Basin (EB), Faroes-Shetland Basin (FSB), Horda Platform (HP), London-Brabant Massif (LBM), Moray Firth Basin (MFB), Møre Basin (MB), Rhenish Massif (RM), Rockall Basin (RB), South Permian Basin (SPB), Unst Basin (UB), West Hebrides Basin (WHP). The mapped extent of the subcrop beneath the 'Mid-Cimmerian Unconformity', which formed due to initiation of the MNSH uplift (Underhill and Partington, 1993) is shown. Depocentres supplied by abundant clastic sediment occur in the Faroes-Shetland Basin (FSB), South Permian Basin (SPB), Egersund Basin (EB) and in northern Germany, in addition to the 'Brent Delta' depocentre in the Viking Graben (VG) and Horda Platform (HP). (**C**) Simplified lithostratigraphic column for the proto-Viking Graben (Fig. 2B) highlighting the main phases of structural evolution in relation to deposition of the Brent Delta sediment routing system(s) (Fig. 3; see text for details).

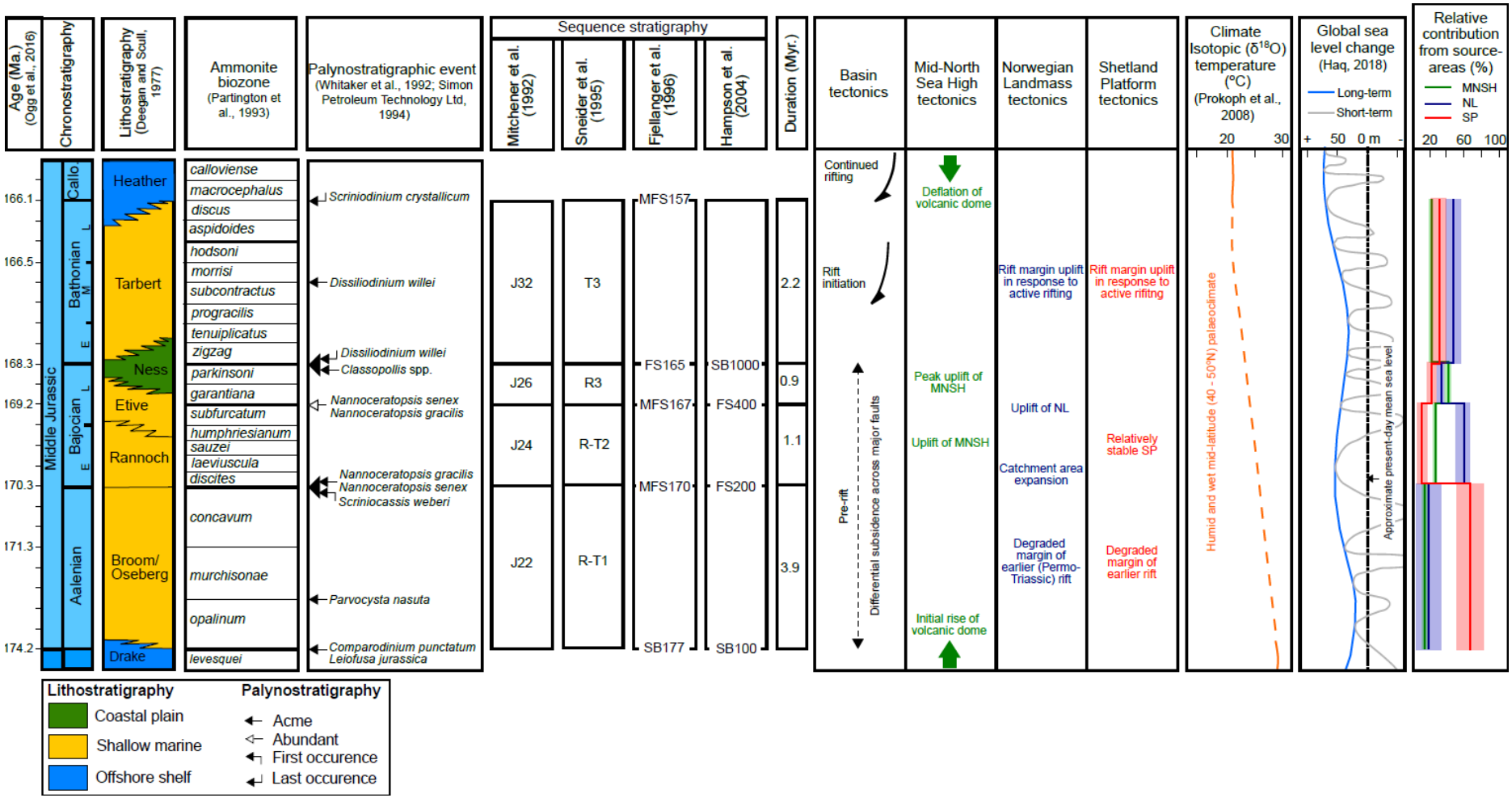

Figure 3. Sequence stratigraphic framework for the 'Brent Delta' sediment routing system(s) synthesised from various published references (Deegan and Scull, 1977; Mitchener et al., 1992; Partington et al., 1993; Sneider et al., 1995; Johannessen et al., 1995; Fjellanger et al., 1996; Hampson et al., 2004). The Aalenian to Bathonian genetic sequences (J22, J24, J26 and J32) of Mitchener

et al. (1992) are used in this study. Possible tectonic drivers in the Shetland Platform, Norwegian Landmass, and Mid-North Sea High source regions and depositional sink, climate (Prokoph et al., 2008), eustatic sea-level change (Haq, 2018), and estimated relative contributions from the source regions to the sediment budget of the ‘Brent Delta’ sediment routing system(s), based on the relative proportion of detrital garnet compositional suites (Morton, 1992), are shown (after Okwara et al., 2023).

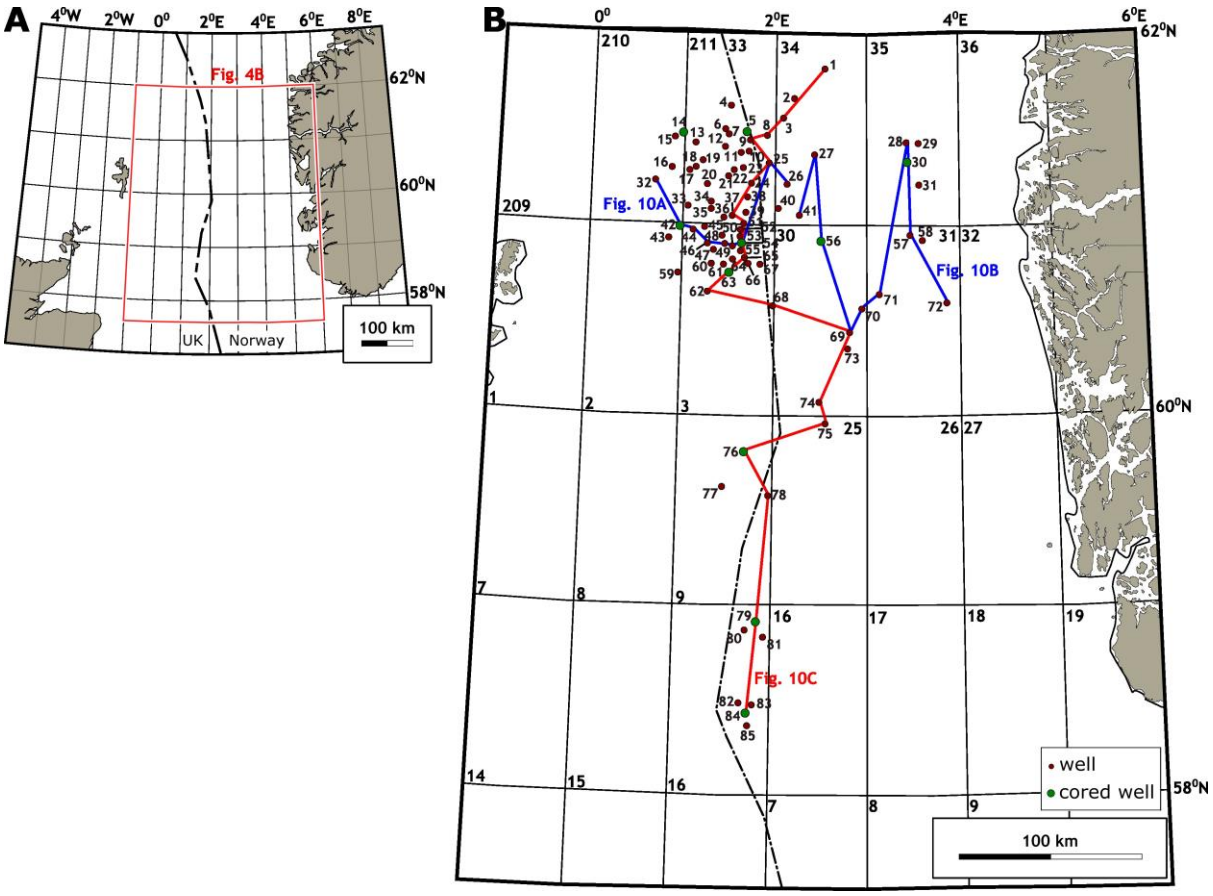

Figure 4. Maps locating: (**A**) the study area (Fig. 4B); and (**B**) wells in the study dataset, and regional stratigraphic correlation panels (Fig. 10). Wells in the study dataset and previously published interpretations of these wells are summarised in Table 1.

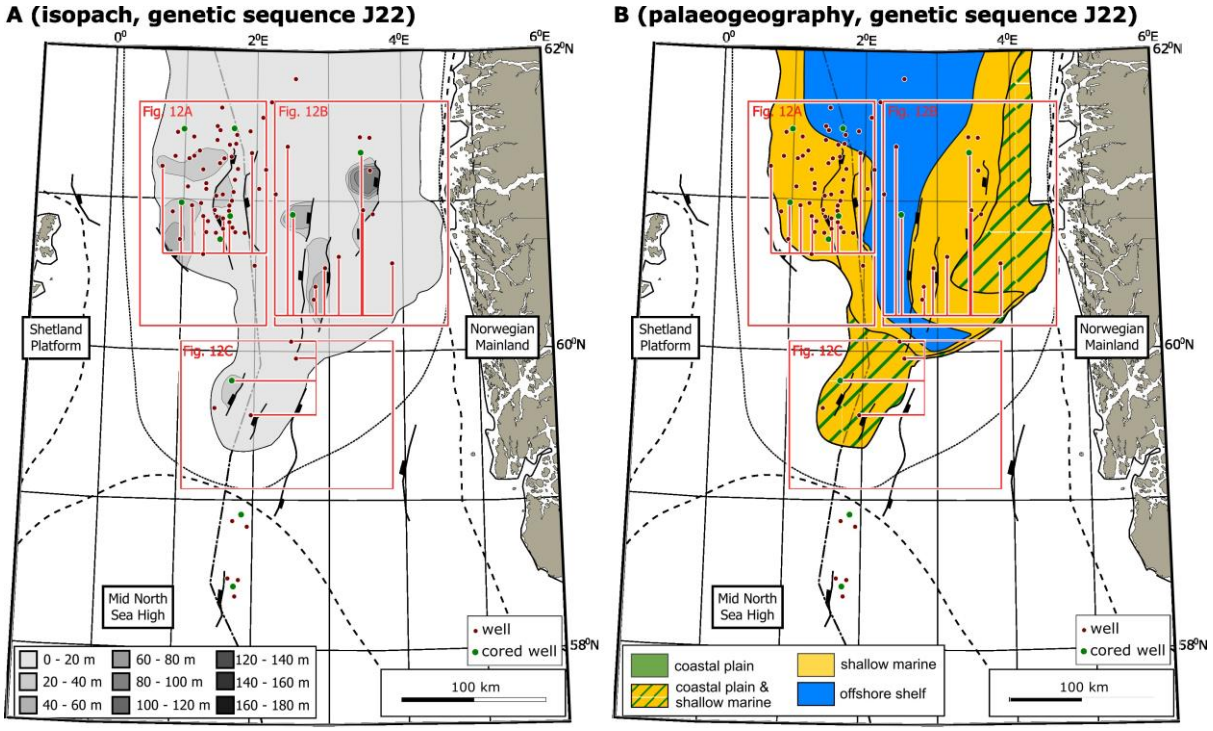

Figure 5. (**A**) Isopach map of undecompacted thickness for genetic sequence J22 (Fig. 3), generated from well data (Fig. 4) and constrained by published isopach maps of Middle Jurassic strata derived from depth-converted seismic data (Mitchener et al., 1992; Husmo et al., 2003). (**B**) Palaeogeographic reconstruction for genetic sequence J22, during maximum progradation of the eastward prograding 'Broom Delta' and westward prograding 'Oseberg Delta' (modified after Mitchener et al., 1992; Fjellanger et al., 1996; Husmo et al., 2003). Maps show the extent of deposition prior to Late Jurassic erosion (dotted lines; Husmo et al., 2003) and the location of Shetland Platform, Norwegian Landmass and Mid-North Sea High source areas (Ziegler 1990; Underhill and Partington, 1993). Cored and uncored wells in the study dataset are shown as green and red circles, respectively. Red rectangles indicate the areas for which sediment masses have been calculated for three distinct sediment routing systems, with wells in each area projected into a transverse (Fig. 12A, B) or axial transect (Fig. 12C) through the sediment routing system.

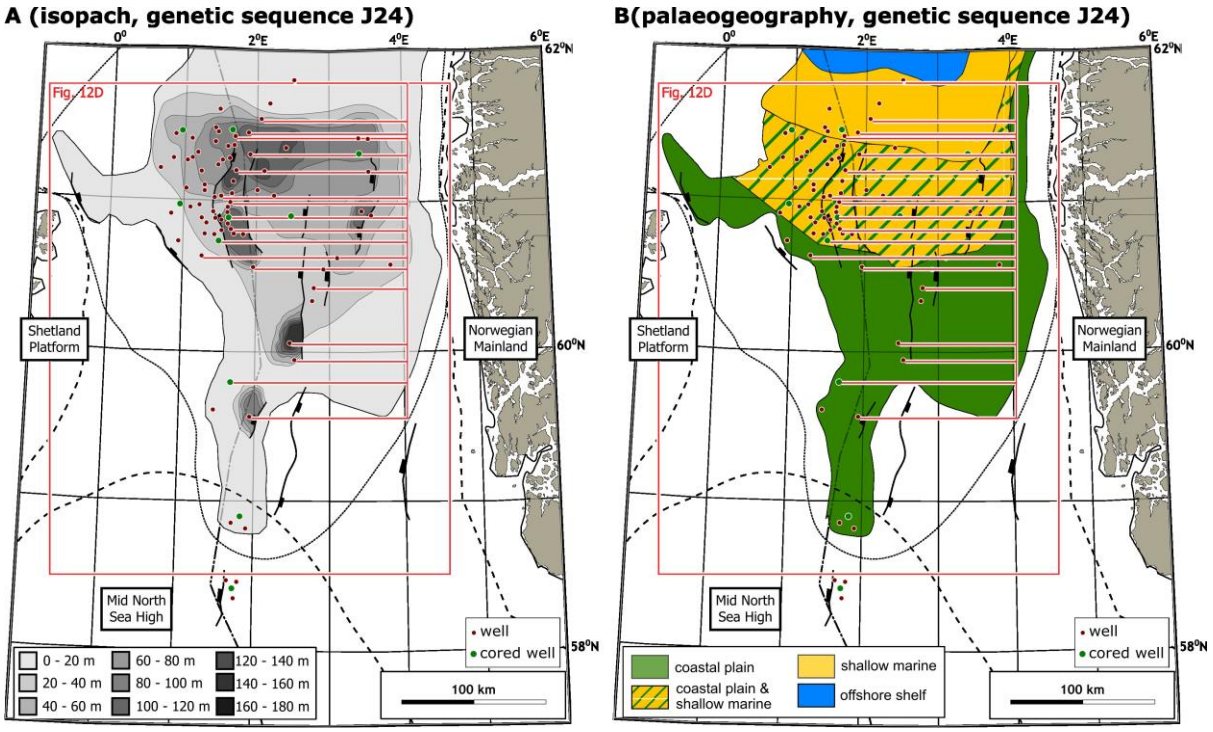

Figure 6. (**A**) Isopach map of undecompacted thickness for genetic sequence J24 (Fig. 3), generated from well data (Fig. 4) and constrained by published isopach maps of Middle Jurassic strata derived from depth-converted seismic data (Mitchener et al., 1992; Husmo et al., 2003). (**B**) Palaeogeographic reconstruction for genetic sequence J24, during maximum progradation of the main, northward-prograding 'Brent Delta' (modified after Mitchener et al., 1992; Fjellanger et al., 1996; Husmo et al., 2003). Maps show the extent of deposition prior to Late Jurassic erosion (dotted lines; Husmo et al., 2003) and the location of Shetland Platform, Norwegian Landmass and Mid-North Sea High source areas (Ziegler 1990; Underhill and Partington, 1993). Cored and uncored wells in the study dataset are shown as green and red circles, respectively. The red rectangle indicates the area for which sediment mass has been calculated for a combined sediment routing system, with wells in the area projected into an axial transect (Fig. 12D) through the sediment routing system.

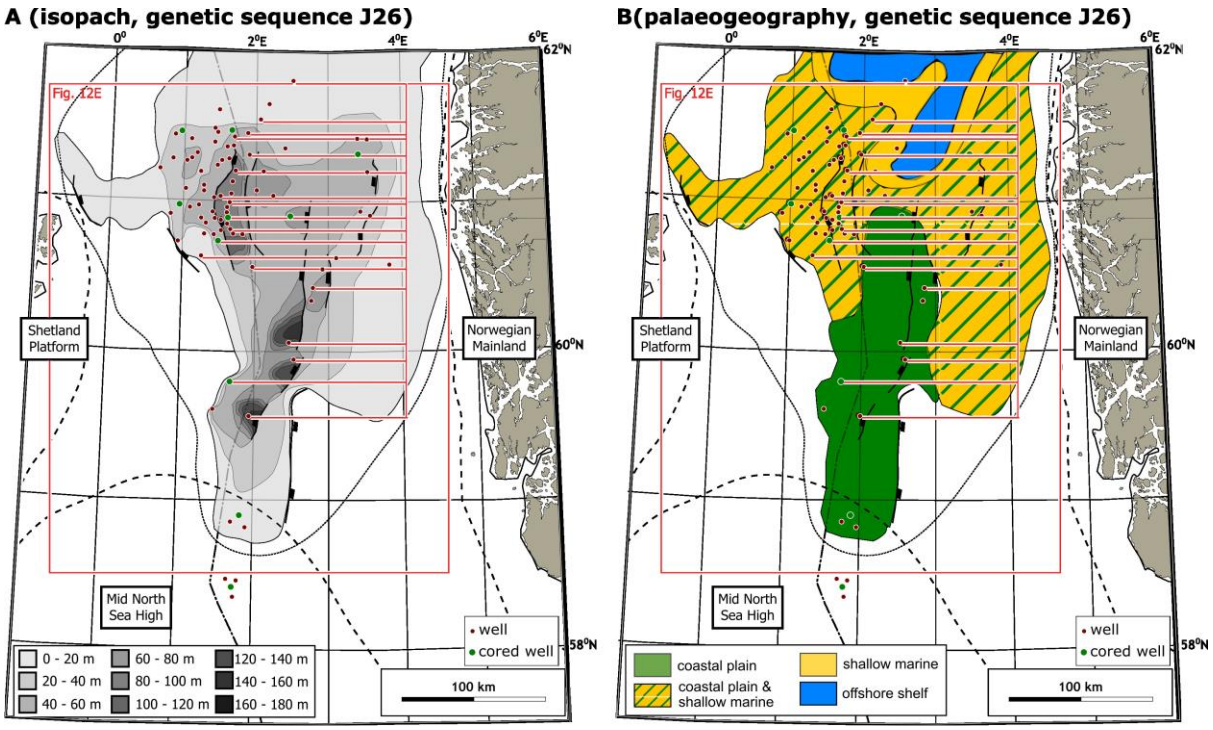

Figure 7. (**A**) Isopach map of undecompacted thickness for genetic sequence J26 (Fig. 3), generated from well data (Fig. 4) and constrained by published isopach maps of Middle Jurassic strata derived from depth-converted seismic data (Mitchener et al., 1992; Husmo et al., 2003). (**B**) Palaeogeographic reconstruction for genetic sequence J26, during aggradation of the main 'Brent Delta' (modified after Mitchener et al., 1992; Fjellanger et al., 1996; Husmo et al., 2003). Maps show the extent of deposition prior to Late Jurassic erosion (dotted lines; Husmo et al., 2002) and the location of Shetland Platform, Norwegian Landmass and Mid-North Sea High source areas (Ziegler 1990; Underhill and Partington, 1993). Cored and uncored wells in the study dataset are shown as green and red circles, respectively. The red rectangle indicates the area for which sediment mass has been calculated for a combined sediment routing system, with wells in the area projected into an axial transect (Fig. 12E) through the sediment routing system.

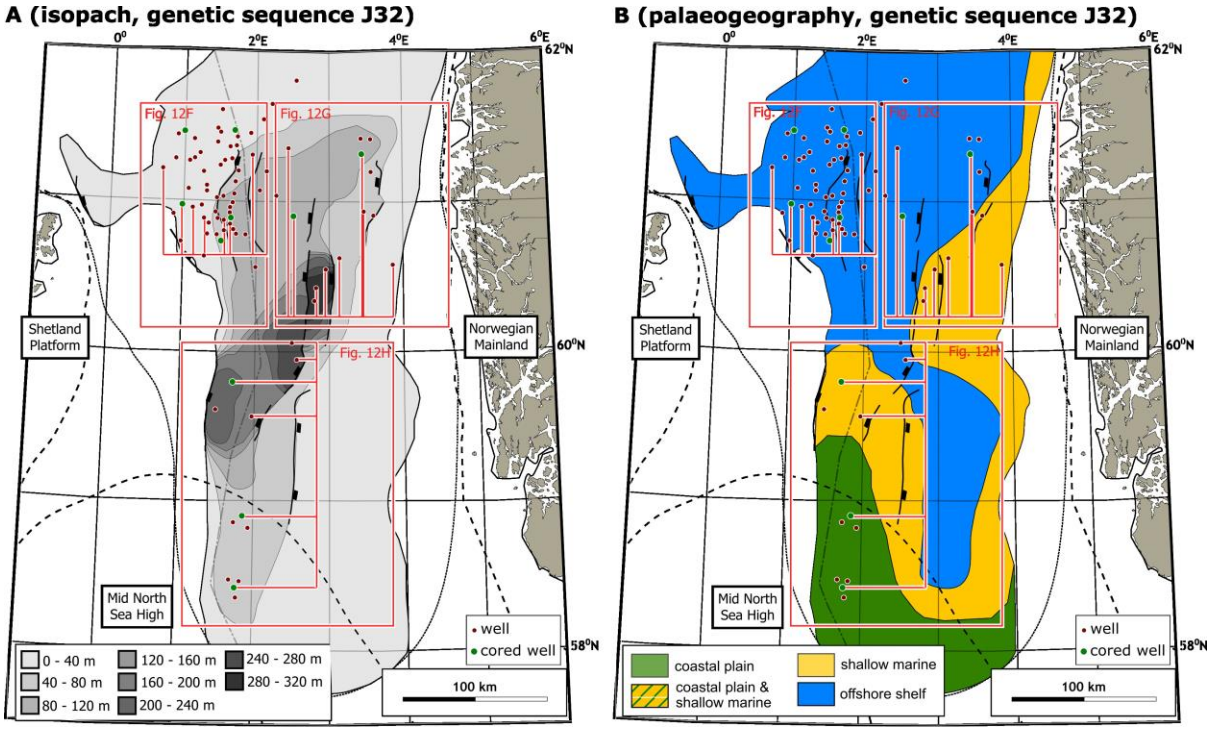

Figure 8. (**A**) Isopach map of undecompacted thickness for genetic sequence J32 (Fig. 3), generated from well data (Fig. 4) and constrained by published isopach maps of Middle Jurassic strata derived from depth-converted seismic data (Mitchener et al., 1992; Husmo et al., 2003). (**B**) Palaeogeographic reconstruction for genetic sequence J32, during transgression and southward retreat of the main 'Brent Delta' (modified after Mitchener et al., 1992; Fjellanger et al., 1996; Husmo et al., 2003). Maps show the extent of deposition prior to Late Jurassic erosion (dotted lines; Husmo et al., 2003) and the location of Shetland Platform, Norwegian Landmass and Mid-North Sea High source areas (Ziegler 1990; Underhill and Partington, 1993). Cored and uncored wells in the study dataset are shown as green and red circles, respectively. Red rectangles indicate the areas for which sediment masses have been calculated for three distinct sediment routing systems, with wells in each area projected into a transverse (Fig. 12F, G) or axial transect (Fig. 12H) through the sediment routing system.

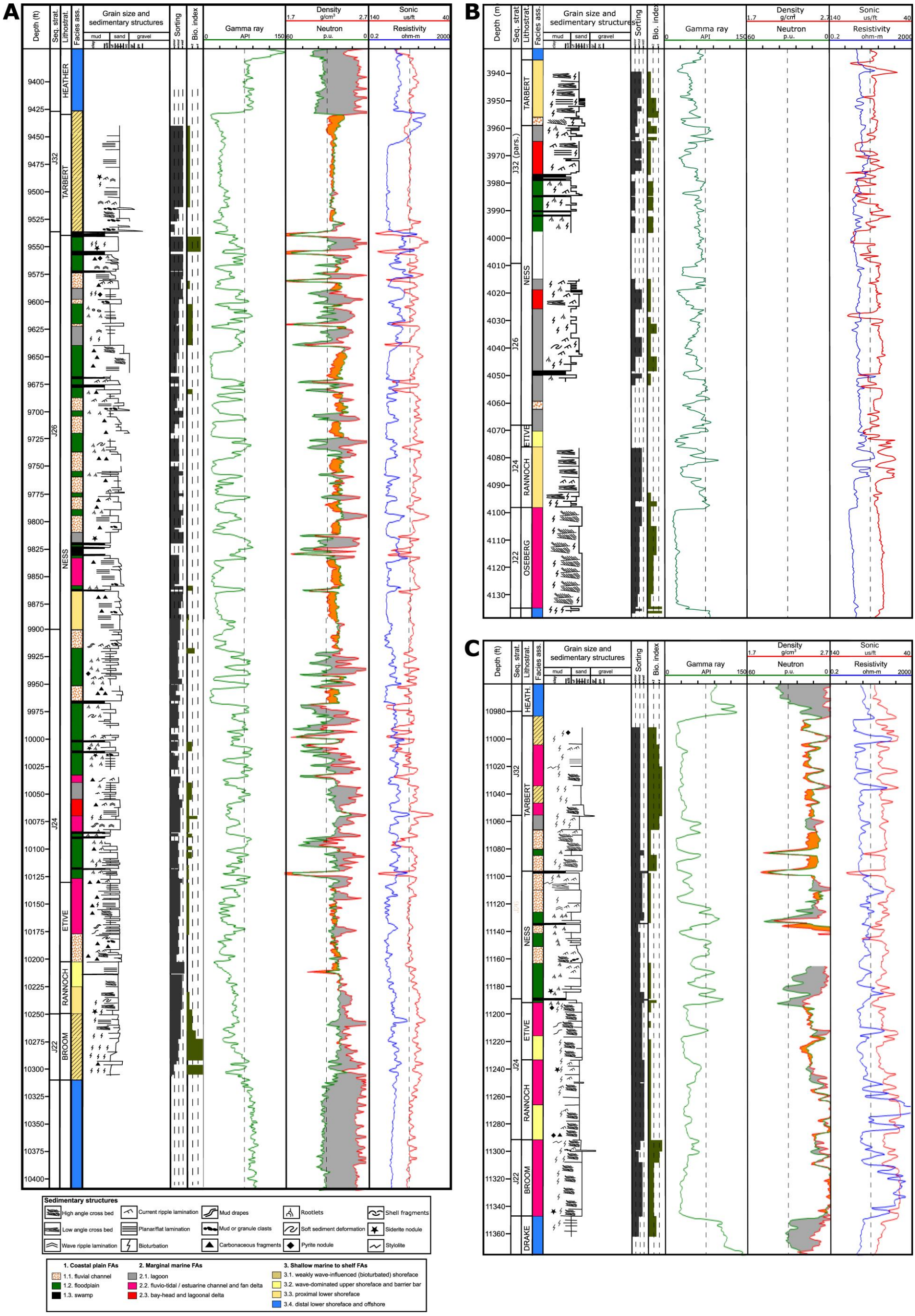
A
B
C
Depth (ft)
Seq. strat.
Lithostrat.
Facies ass.
Grain size and sedimentary structures
mud
sand
gravel
Sorting
Bio. index
Gamma ray
API
Density
g/cm3
Neutron
p.u.
Sonic
us/ft
Resistivity
ohm-m
HEATHER
TARBERT
NESS
ETIVE
RANNOCH
BROOM
DRAKE
J32
J26
J24
J22
J32 (pars.)
OSEBERG
Sedimentary structures
High angle cross bed
Low angle cross bed
Wave ripple lamination
Current ripple lamination
Planar/flat lamination
Bioturbation
Mud drapes
Mud or granule clasts
Carbonaceous fragments
Rootlets
Soft sediment deformation
Pyrite nodule
Shell fragments
Siderite nodule
Stylolite
1. Coastal plain FAs
1.1. fluvial channel
1.2. floodplain
1.3. swamp
2. Marginal marine FAs
2.1. lagoon
2.2. fluvio-tidal / estuarine channel and fan delta
2.3. bay-head and lagoonal delta
3. Shallow marine to shelf FAs
3.1. weakly wave-influenced (bioturbated) shoreface
3.2. wave-dominated upper shoreface and barrier bar
3.3. proximal lower shoreface
3.4. distal lower shoreface and offshore

Figure 9. Sedimentological core logs and wireline logs of representative wells from the Brent Delta routing system(s): (**A**) well 3/4a-12, Strathspey Field, offshore UK; (**B**) well 30/2-2, Huldra Field, offshore Norway; and (**C**) well 2/5-3, Heather Field, offshore UK (Table 2, Fig. 4; after Okwara et al., 2023). Core-defined facies associations (Table 3) are calibrated to wireline logs. Orange and grey colours in neutron-density log track indicate ‘sand cross over’ and ‘shale cross over’, respectively. Sequence stratigraphic divisions are synthesised from published literature (Fig. 3; see text for details).

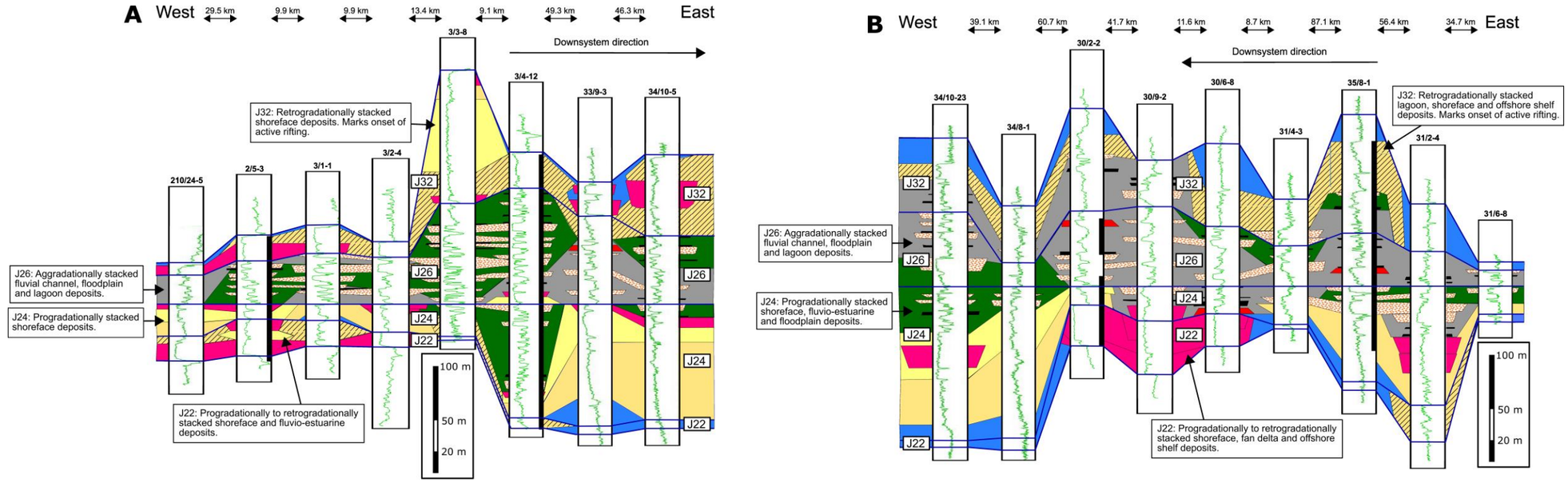
A West
29.5 km
9.9 km
9.9 km
13.4 km
9.1 km
49.3 km
46.3 km
East
Downsystem direction
3/3-8
3/4-12
33/9-3
34/10-5
3/2-4
3/1-1
2/5-3
210/24-5
J32: Retrogradationally stacked shoreface deposits. Marks onset of active rifting.
J26: Aggradationally stacked fluvial channel, floodplain and lagoon deposits.
J24: Progradationally stacked shoreface deposits.
J22: Progradationally to retrogradationally stacked shoreface and fluvio-estuarine deposits.
J32
J26
J24
J22
100 m
50 m
20 m
B West
39.1 km
60.7 km
41.7 km
11.6 km
8.7 km
87.1 km
56.4 km
34.7 km
East
Downsystem direction
30/2-2
34/10-23
34/8-1
30/9-2
30/6-8
31/4-3
35/8-1
31/2-4
31/6-8
J32: Retrogradationally stacked lagoon, shoreface and offshore shelf deposits. Marks onset of active rifting.
J26: Aggradationally stacked fluvial channel, floodplain and lagoon deposits.
J24: Progradationally stacked shoreface, fluvio-estuarine and floodplain deposits.
J22: Progradationally to retrogradationally stacked shoreface, fan delta and offshore shelf deposits.
J32
J26
J24
J22
100 m
50 m
20 m
C South
50.2 km
81.1 km
24.2 km
56.5 km
16.5 km
49.3 km
46.3 km
37.9 km
16.3 km
11.0 km
11.5 km
9.0 km
16.8 km
20.8 km
14.8 km
15.7 km
10.3 km
22.9 km
32.6 km
North
1. Coastal plain FAs
1.1. fluvial channel
1.2. floodplain
1.3. swamp
2. Marginal marine FAs
2.1. lagoon
2.2. fluvio-tidal / estuarine channel and fan delta
2.3. bay-head and lagoonal delta
3. Shallow marine to shelf FAs
3.1. weakly wave-influenced (bioturbaed) shoreface
3.2. wave-dominated upper shoreface and barrier bar
3.3. proximal lower shoreface
3.4. distal lower shoreface and offshore
Downsystem direction
15/9-2
15/3-3
24/6-1
9/9-3
25/2-7
30/11-3
3/8-10
3/9-4
3/4-12
211/28-5
211/24-4
33/9-3
211/19-3
33/9-14
34/4-3
34/2-4
30/9-2
29/6-1
3/12-2
3/4-1
Sleipner Formation
Bruce - Upper Sands
Bruce - A
Bruce - B
Bruce - C
Tarbert
Ness Formation
Etive
Rannoch
Broom
Fault terrace with expressed inherited topography?
Onlap on Triassic? basement during J32 transgression
J32: Retrogradationally stacked shoreface deposits. Marks onset of active rifting.
J26: Aggradationally stacked fluvial channel and floodplain deposits.
J22: Progradationally to retrogradationally stacked shoreface and fluvio-estuarine deposits.
J24: Progradationally stacked shoreface deposits.
Rapid northward thinning of all units towards downsystem termination?
J32
J26
J24
J22
100 m
50 m
20 m

Figure 10. Regional sequence stratigraphic correlation panels: (**A**) transverse panel from the western basin margin, adjacent to the Shetland Platform source area, to the basin centre; (**B**) transverse panel from the eastern basin margin, adjacent to the Norwegian Landmass source area, to the basin centre; and (**C**) axial panel from the southern basin margin, adjacent to the Mid North Sea High source area, to the northern limit of the basin (after Mitchener et al., 1992; Sneider et al., 1995; Fjellanger et al., 1996; Hampson et al., 2004; Okwara et al., 2023). Panels are located in Figure 4, and flattened on the top of the J24 genetic sequence. Given the large well spacing, only stratigraphic surfaces bounding genetic sequences J22, J24, J26 and J32 (Fig. 3) are shown.

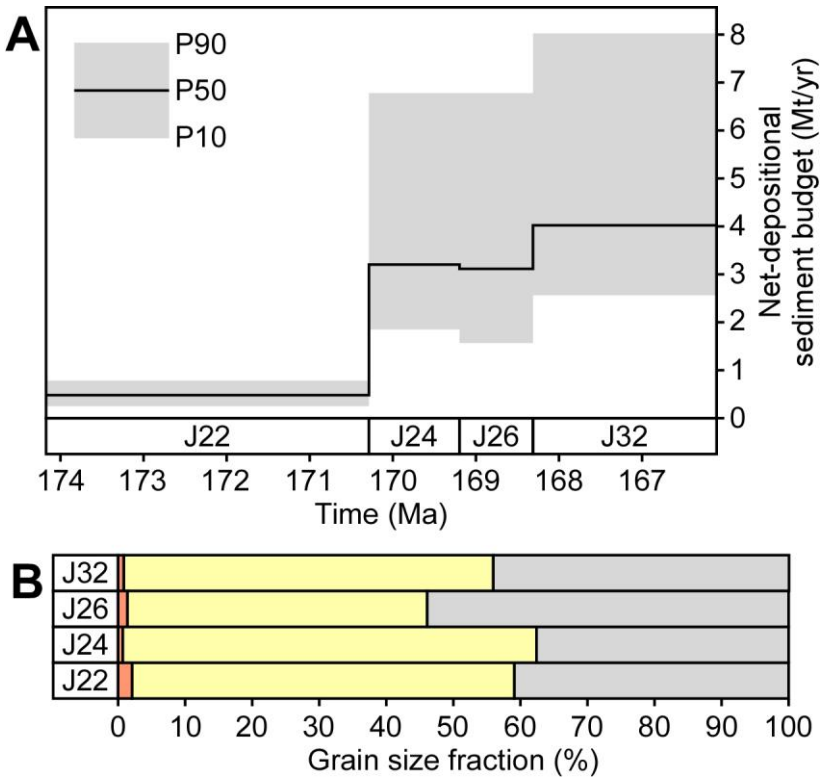

Figure 11. (**A**) Net-depositional sediment budget for the four genetic sequences of the 'Brent Delta' sediment routing system(s) (Fig. 3; after Okwara et al., 2023). Genetic sequences are shown from oldest (J22, left) to youngest (J32, right). Black line shows the median (P50) value and grey shading shows the 10th to 90th percentile range (P10-P90) for each genetic sequence. (**B**) Proportion of grain-size classes (gravel, sandstone and mudstone) by mass in genetic sequences J22, J24, J26 and J32, based on mapped sediment volumes (Figs. 5-8) that are subdivided into facies proportions in 84 representative wells (Figs. 4, 9). Each facies is assigned a specific grain size composition (Table 3) and volume-to-mass conversions based on density log data are applied to each grain-size class (2400 kg m^{-3} = gravel conglomerate and sandstone bulk density, 2500 kg m^{-3} = mudstone bulk density; Okwara et al., 2023).

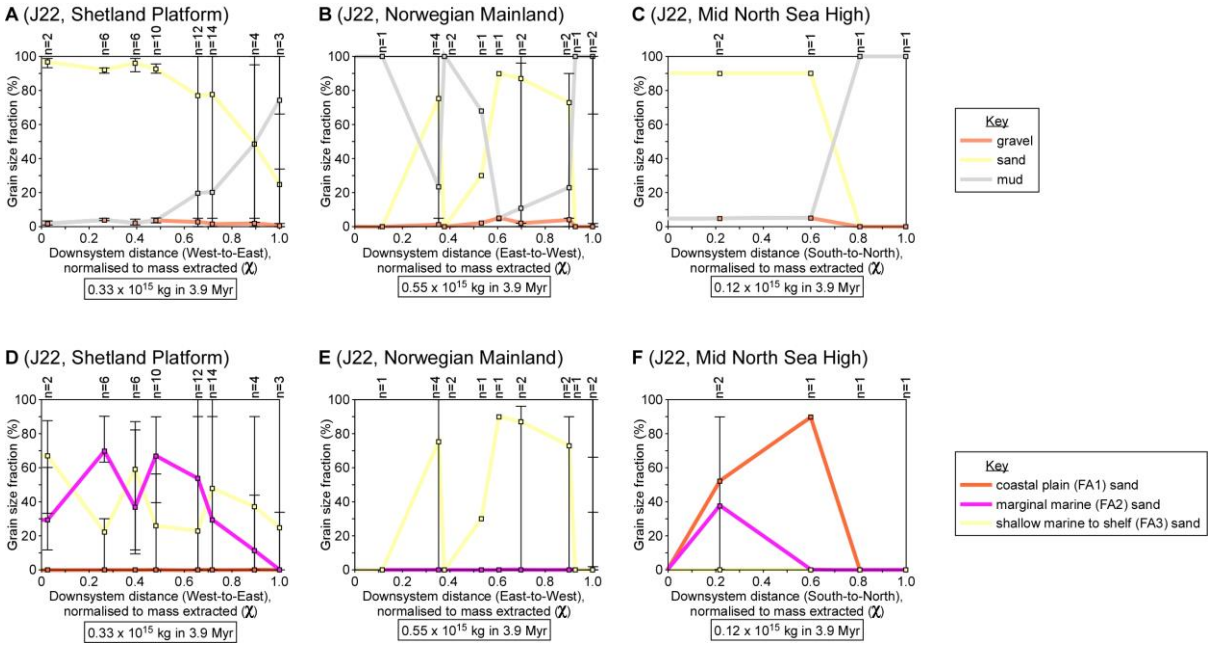

Figure 12. Downsystem variations in (**A-C**) percentage-thickness of gravel, sandstone and mudstone, and (**D-F**) percentage-thickness of coastal-plain, marginal-marine and shallow-marine sandstones for genetic sequence J22 (cf. Figs. 5, 10A-C) in the study well database (Fig. 4), as a function of sediment mass extracted (χ) (Fig. 1). Downsystem variations are shown for: (**A, D**) transverse transect for western basin margin, sourced from Shetland Platform; (**B, E**) transverse transect for eastern basin margin, sourced from Norwegian Landmass; and (**C, F**) axial transect for southern basin margin, sourced from Mid-North Sea High (Fig. 5). Each point in the plots represents the mean value for a group of wells located at a specific downsystem distance, with the number of wells in the group indicated at the top of the plot (e.g. “n=3”). The vertical error bar for each point shows the variation in percentage-thickness values between wells in the group.

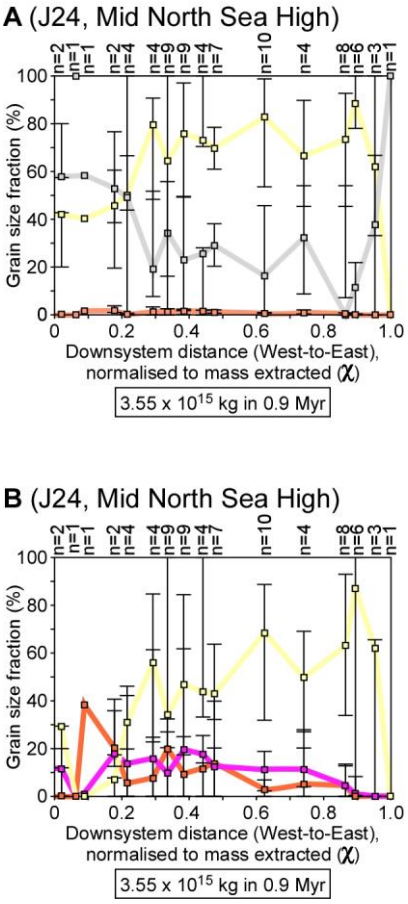

Figure 13. Downsystem variations in (**A**) percentage-thickness of gravel, sandstone and mudstone, and (**B**) percentage-thickness of coastal-plain, marginal-marine and shallow-marine sandstones for genetic sequence J24 (cf. Figs. 6, 10C) in the study well database (Fig. 4), as a function of sediment mass extracted (χ) (Fig. 1). Downsystem variations are shown for axial transect along basin centre, sourced from Shetland Platform, Norwegian Landmass and Mid-North Sea High (Fig. 6). Each point in the plots represents the mean value for a group of wells located at a specific downsystem distance, with the number of wells in the group indicated at the top of the plot (e.g. “n=3”). The vertical error bar for each point shows the variation in percentage-thickness values between wells in the group.
Key as for Figure 12.

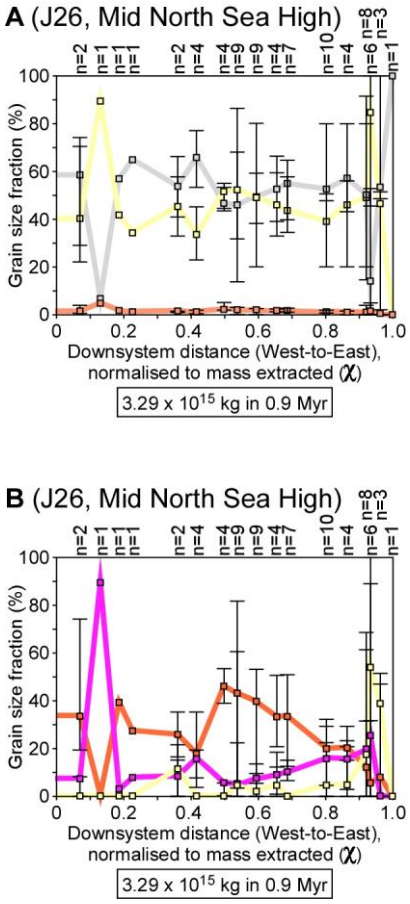

Figure 14. Downsystem variations in (A) percentage-thickness of gravel, sandstone and mudstone, and (B) percentage-thickness of coastal-plain, marginal-marine and shallow-marine sandstones for genetic sequence J26 (cf. Figs. 7, 10C) in the study well database (Fig. 4), as a function of sediment mass extracted (χ) (Fig. 1). Downsystem variations are shown for axial transect along basin centre, sourced from Shetland Platform, Norwegian Landmass and Mid-North Sea High (Fig. 7). Each point in the plots represents the mean value for a group of wells located at a specific downsystem distance, with the number of wells in the group indicated at the top of the plot (e.g. “n=3”). The vertical error bar for each point shows the variation in percentage-thickness values between wells in the group.
Key as for Figure 12.

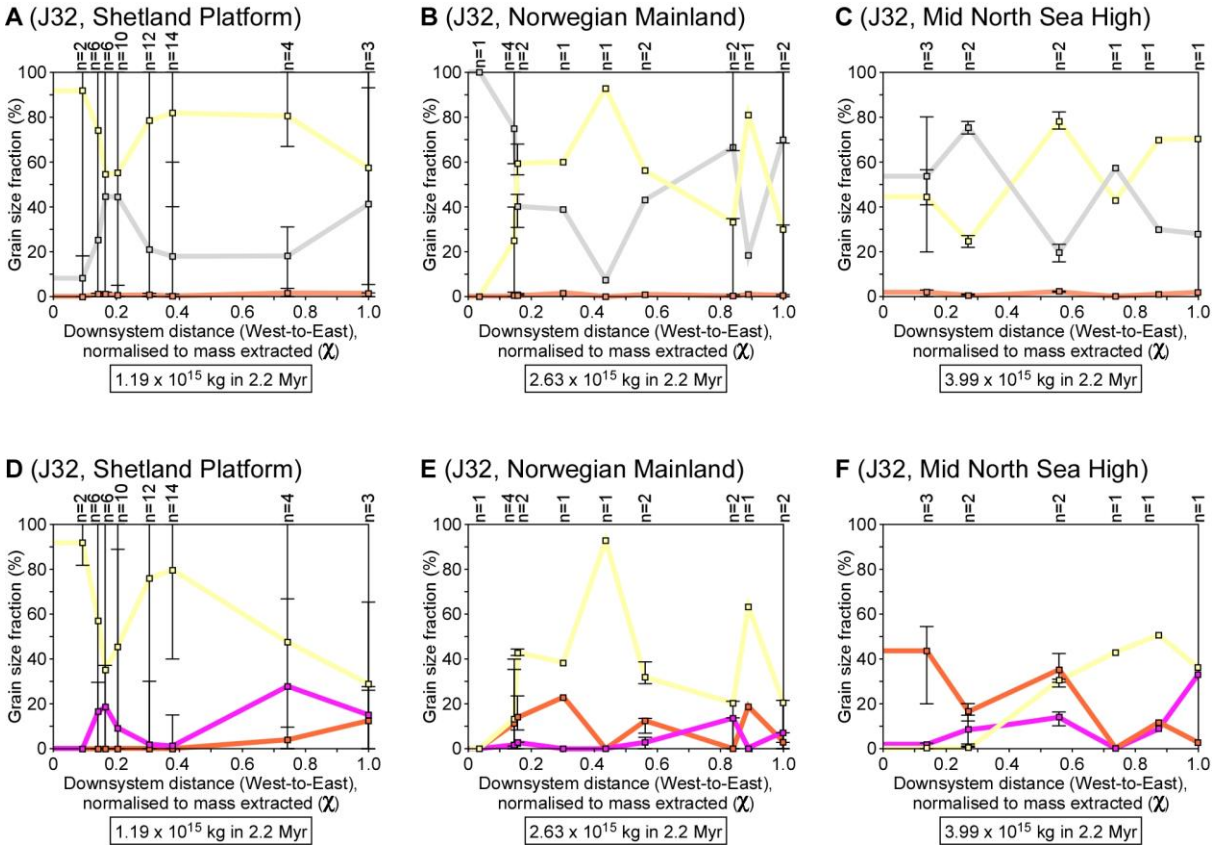

Figure 15. Downsystem variations in (**A-C**) percentage-thickness of gravel, sandstone and mudstone, and (**D-F**) percentage-thickness of coastal-plain, marginal-marine and shallow-marine sandstones for genetic sequence J32 (cf. Figs. 8, 10A-C) in the study well database (Fig. 4), as a function of sediment mass extracted (χ) (Fig. 1). Downsystem variations are shown for: (**A, D**) transverse transect for western basin margin, sourced from Shetland Platform; (**B, E**) transverse transect for eastern basin margin, sourced from Norwegian Landmass; and (**C, F**) axial transect for southern basin margin, sourced from Mid-North Sea High (Fig. 8). Each point in the plots represents the mean value for a group of wells located at a specific downsystem distance, with the number of wells in the group indicated at the top of the plot (e.g. “n=3”). The vertical error bar for each point shows the variation in percentage-thickness values between wells in the group.
Key as for Figure 12.

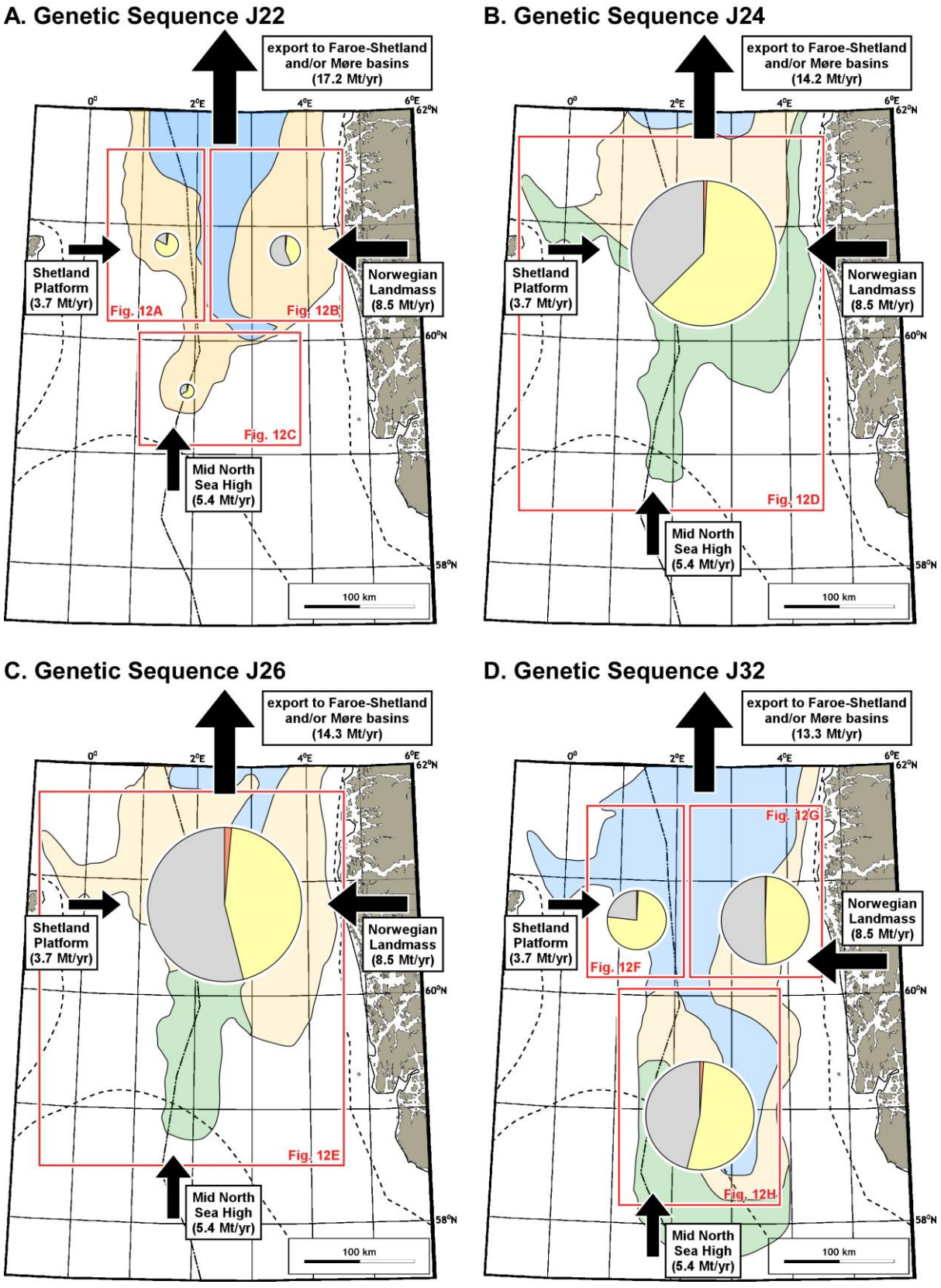

Figure 16. Maps illustrating partitioning of sediment mass by grain-size fraction for: (**A**) transverse and axial sediment routes in genetic sequence J22 (Figs. 5, 10A-C,

12); (**B**) combined transverse-and-axial sediment route in genetic sequence J24 (Figs. 6, 10A-C, 13); (**C**) combined transverse-and-axial sediment route in genetic sequence J26 (Figs. 7, 10A-C, 14); and (**D**) transverse and axial sediment routes in genetic sequence J32 (Figs. 8, 10A-C, 15). Pie charts for each transverse, axial and combined transverse-and-axial sediment route are scaled by area according to the rate of net deposition by sediment mass, with coloured segments indicating the proportions of gravel (orange), sand (yellow) and mud (grey) (cf. Fig. 11B). Black arrows indicate fluvial sediment supply rates (influx) from the Shetland Platform, Norwegian Landmass and Mid-North Sea High source areas, estimated using the BQART model (Okwara et al., 2023), and sediment bypass rates (efflux) to the Faroe-Shetland Basin and/or western Møre Basin, estimated as the sum of the BQART-derived influxes minus net-depositional rate in the 'Brent Delta' sediment routing system(s) (i.e. pie charts). Values of BQART-derived fluvial sediment supply rates are estimated over the entire duration of Brent Group deposition (i.e. averaged over genetic sequences J22, J24, J26 and J32).

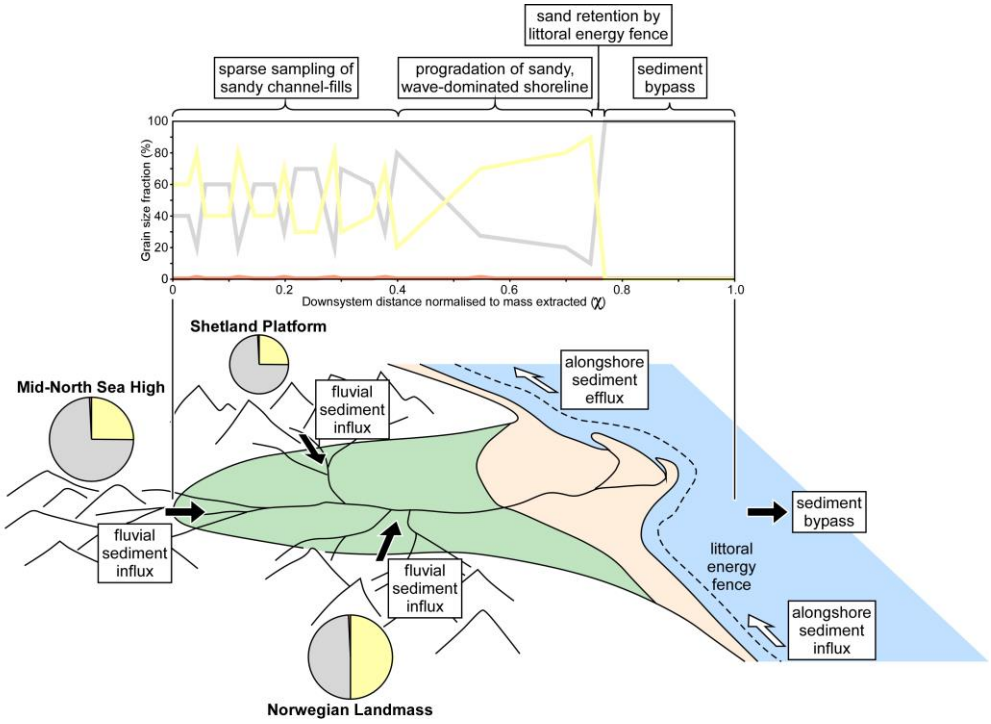

Figure 17. Conceptual model synthesising sediment source regions, sediment influxes and effluxes, depositional environments, and downsystem variations in gravel (orange), sandstone (yellow) and mudstone (grey) in the axial ‘Brent Delta’ sediment routing system. See text for discussion.